

JGR Solid Earth

RESEARCH ARTICLE

10.1029/2024JB029677

Key Points:

- A new Antarctic lithosphere model is derived by seismic-constrained gravity inversion
- The impact of heterogeneous composition for estimating mantle temperature is quantified
- Mantle viscosity, lithosphere thickness, and geothermal heat flow are derived from the updated mantle thermal structure

Supporting Information:

Supporting Information may be found in the online version of this article.

Correspondence to:

L. Li,
lu.li@csiro.au

Citation:

Li, L., Aitken, A. R. A., Gross, L., & Codd, A. (2025). Resolving mantle composition suggests a warmer East Antarctic mantle. *Journal of Geophysical Research: Solid Earth*, 130, e2024JB029677. <https://doi.org/10.1029/2024JB029677>

Received 7 JUN 2024

Accepted 18 FEB 2025

Author Contributions:

Conceptualization: Lu Li, Alan R. A. Aitken, Lutz Gross

Data curation: Lu Li

Formal analysis: Lu Li

Funding acquisition: Alan R. A. Aitken

Investigation: Lu Li, Alan R. A. Aitken, Lutz Gross, Andrea Codd

Methodology: Lu Li, Alan R. A. Aitken, Lutz Gross, Andrea Codd

Project administration: Lu Li, Alan R. A. Aitken

Resources: Lu Li, Alan R. A. Aitken, Lutz Gross

Software: Lu Li, Lutz Gross, Andrea Codd

Supervision: Alan R. A. Aitken

Validation: Lu Li, Alan R. A. Aitken

Visualization: Lu Li

Writing – original draft: Lu Li, Alan R. A. Aitken

© 2025. The Author(s).

This is an open access article under the terms of the [Creative Commons Attribution License](#), which permits use, distribution and reproduction in any medium, provided the original work is properly cited.

Resolving Mantle Composition Suggests a Warmer East Antarctic Mantle

Lu Li^{1,2,3} , Alan R. A. Aitken^{1,2} , Lutz Gross⁴ , and Andrea Codd⁴ 

¹School of Earth and Oceans, The University of Western Australia, Perth, WA, Australia, ²Australian Centre of Excellence for Antarctic Science, The University of Western Australia, Perth, WA, Australia, ³Now at Mineral Resources, CSIRO, Kensington, WA, Australia, ⁴School of Mathematics and Physics, The University of Queensland, Brisbane, QLD, Australia

Abstract Antarctica's geothermal heat flow and its glacial isostatic adjustment response are critical to understand ice sheet stability. These demand a knowledge of the temperature of the Antarctic lithosphere, but challenges remain in resolving mantle thermomechanical properties. Here we use a two-stage process to resolve mantle temperature and composition. First, we derive an optimized relationship between shear-wave velocity and temperature, density, and composition, constrained by temperature, attenuation, and the average viscosity of the oceanic upper mantle. Applying this conversion relationship to a seismic shear-wave velocity model from adjoint tomography (ANT-20) yields an estimate of mantle density and temperature. In the second stage we apply a 3D finite-element-method gravity inversion to correct density distribution for the Antarctic lithosphere. The updated density structure further constrains the composition and so the temperature of the lithospheric mantle. Factoring in changes in mantle composition, areas with depleted mantle require a higher temperature than the initial estimate to fit the seismic velocity and density structure. Compared with a primitive mantle, the temperature in the depleted mantle is increased by up to 200°C. From the updated temperature field, changes to the lithosphere thickness, mantle viscosity, and geothermal heat flow are defined: in East Antarctica, the low viscosity area is largely unchanged (<10²³ Pa s), while the estimated lithosphere thickness must decrease by up to 150 km, and heat flow must increase by 3–10 mW/m². Collectively, the effects of an increased mantle temperature estimate suggest that a more dynamic and climate-responsive East Antarctic Ice Sheet is possible.

Plain Language Summary Temperature variations in the mantle provide differences in the heat supplied to the Earth surface, and also control mantle flow, influencing the rate of land uplift caused by the loss of ice mass. These two factors are crucial conditions for ice sheet flow, but they are poorly resolved in Antarctica. Seismic-wave speeds provide the capability to estimate the mantle temperature field but the velocity to temperature relationship is not straightforward. In a two-stage process we first resolve how seismic shear wave speed varies with temperature, pressure and chemical composition. This relationship allows us to estimate the temperature and density of the mantle, reflecting variations in iron and magnesium content. In a second stage gravity measurements are used to correct the density distribution in the mantle and redefine the mantle temperature and composition to satisfy both the seismic-wave speed and the revised density. We find that the mantle in East Antarctica is up to 200°C hotter than previously estimated, as variations in chemical composition were not included in earlier models. The mantle temperature field is used to map variations of the lithosphere's thickness, the mantle's viscosity, and the conduction of heat from the mantle to the Earth surface.

1. Introduction

The mantle thermal structure contributes up to 50 mW/m² to Antarctic geothermal heat flow (GHF) and determines mantle viscosity, which impacts the long-term stability of the Antarctic ice sheet (Noble et al., 2020). Geothermal heat warms the base of the ice sheet, influences ice rheology, including melting, and forms an important basal boundary condition for ice sheet dynamics (Burton-Johnson et al., 2020; Reading et al., 2022). The inaccessibility of the ice sheet bed makes geothermal heat flow one of the least constrained basal boundary conditions (Llubes et al., 2006). The thickness of lithosphere and viscosity of the upper mantle control how fast the lithosphere responds to ice sheet mass changes through Glacial-Isostatic-Adjustment (GIA) related uplift of bedrock. Rapid uplift could temporarily stabilize parts of the West Antarctic Ice Sheet after ice loss (Barletta et al., 2018), but such rapid uplift is considered less likely in East Antarctica, where the mantle is modeled to be much colder, thicker, and more viscous. Therefore, precise modeling of the mantle thermal structure is a key requirement for predicting the dynamics of the Antarctic Ice Sheet and its impact on future sea level rise.

Writing – review & editing: Lu Li, Alan R. Aitken, Lutz Gross, Andrea Codd

The current understanding of the continental-scale mantle thermal structure relies on linking geophysical data with thermal parameters determined by the mantle chemical composition (Stixrude & Lithgow-Bertelloni, 2005, 2011). Seismic velocity models are widely used to resolve the mantle thermal structure, possible because thermal effects dominate seismic velocity changes. Converting a seismic velocity model into a temperature model requires knowledge of the shear modulus and seismic attenuation. This can be achieved through a forward mineral physics approach that uses mineral assembly of the mantle chemical composition. Such an approach requires extrapolation of mineral physics parameters from laboratory measurements to mantle conditions (Cammarano et al., 2003; Goes et al., 2000). Due to the limited geological knowledge beneath ice sheets, a homogeneous mantle composition is commonly assumed to convert seismic velocity into temperature in Antarctica. For example, An et al. (2015) utilized a non-cratonic lithospheric composition to convert shear-wave velocity into temperature. Their results revealed the first-order thermal condition in the lithospheric mantle, with a warm and thin lithosphere in West Antarctica and a thick and cold lithosphere in East Antarctica. Although seismic velocity alone can constrain large-scale thermal variations, the uncertainties of the resolved temperature model may reach several hundreds of degrees centigrade (Feng et al., 2010). Thus, additional information is necessary to fully represent the thermal structure, including the ability to determine absolute mantle temperatures and to assess the impact of compositional heterogeneity.

In most cases, mineral physical parameters are challenging to match with the applied seismic velocity model. This discrepancy arises due to the difficulty in determining the amplitude of seismic velocity variations, which is subjected to the choice of initial reference model, attenuation, and the applied regularization during the inversion process (Foulger et al., 2013). In the meantime, the mineral physical parameters are required to extrapolate several orders of magnitude from lab conditions to the mantle conditions. Consequently, only the relative temperature change can be resolved, failing to constrain the absolute temperature, which then limits its capacity to model geothermal heat flow (Haeger et al., 2022). One way to mitigate this challenge is by using areas with well-constrained seismic velocity-temperature-pressure relationships to re-estimate parameters that impact shear modulus and attenuation. In Antarctica, Hazzard et al. (2023) used temperatures in the oceanic lithosphere to estimate the shear wave velocity and temperature conversion relationship. This approach can be seen as using an average bulk composition of the oceanic lithosphere to represent the Antarctic continent and the Southern Ocean. However, evidence from limited rock outcrops, seismic tomography models, and multivariable analyses indicates that the composition of the Antarctic lithosphere is highly heterogeneous (Cox et al., 2023; Schaeffer & Lebedev, 2015; Stål et al., 2019), with a significant portion of East Antarctica displaying an Archean to Proterozoic cratonic-type lithosphere (Boger, 2011; Cox et al., 2023; Schaeffer & Lebedev, 2015). Therefore, to fully resolve mantle temperature, we must consider mantle composition heterogeneity, although the current framework has limited capacity to achieve this.

Based on mineral physical parameters, variations in both temperature and chemical composition can impact seismic velocity and density. Thus, to address composition heterogeneity, gravity data, that resolves density distribution, can be added to the workflow (Afonso et al., 2013, 2016, 2022; Fullea et al., 2009, 2021; Haeger et al., 2019; Pappa et al., 2019). In Antarctica, Haeger et al. (2019) used an iterative approach to resolve variations in both temperature and composition constrained by a seismic velocity model and gravity data. Their results indicate that considering composition variation is necessary to constrain the thermal structure in East Antarctica. However, because the composition impact on the shear-wave velocity relationship is adapted using a mineral-physical approach, their results cannot determine the absolute temperature in the mantle (Haeger et al., 2022). This limits a direct application for resolving geothermal heat flow and mantle viscosity.

To address the challenge to constrain the absolute mantle temperature while fully accounting for compositional heterogeneity, we applied a two-stage method. In the first stage, we modified the calibrated temperature-density-shear-wave velocity relationship from Hazzard et al. (2023) by introducing a composition term to account for compositional variations; In the second stage, benefiting from the ability of gravity to resolve the compositional signal of the lithosphere, we generated a high-resolution model including 3D lithosphere density based on the shear-wave velocity model ANT-20 (Lloyd et al., 2020) and detailed crustal structure (Li & Aitken, 2024). A 3D gravity inversion utilized a novel preconditioned conjugate gradient method with an unstructured mesh to update the crust and upper mantle density distribution (Codd et al., 2021). The density results are used to generate an updated temperature and compositional structure of the mantle that satisfies both the seismic and gravity constraints. The updated temperature field is used to estimate lithosphere thickness, mantle viscosity, and geothermal heat flow.

2. Tectonic Setting

Antarctica is a geologically complex region, and its tectonic history is poorly understood due to its remote location and the fact that much of the geological information is hidden beneath the ice sheet. Antarctica is commonly divided into East Antarctica and West Antarctica along the Transantarctic Mountains (Dalziel & Lawver, 2001), with different tectonic histories and physical properties. However, recent observations and models suggest a more complex view of tectonic boundaries (Jordan et al., 2022; Stål et al., 2019; Tankersley et al., 2022; Tinto et al., 2019).

East Antarctica is characterized by Archean to Proterozoic age lithosphere based on outcrops (Cox et al., 2019). Seismic structure in this region generally exhibits faster velocities than the reference tomography model (Figure 1b). Several regions exhibit extremely fast velocities, such as the center of EANT to the Wilkes Subglacial Basin region, and Princess Elizabeth Land (PEL), which are 4%–8% faster than the reference velocity model (STW105, Kustowski et al. (2008)), indicating a cold and dense lithosphere with probably different composition (Lloyd et al., 2020).

East Antarctica contains rift systems, large suture zones, and several cratonic blocks that link to the formation and break of supercontinents (Aitken et al., 2014, 2016; Boger, 2011; Ferraccioli et al., 2011; Jordan et al., 2022). The Lambert Rift system is marked as a Mesozoic failed rift system with two distinct phases (Lisker et al., 2003). The early denudation phase in the late Paleozoic is linked to the formation of the graben, and the later denudation phase in the early Cretaceous phase might be linked to the initial separation of the Indian and Antarctica (Lisker et al., 2003). A large suture zone (Indo-Australo-Antarctic Suture) is suggested in the Aurora Subglacial Basin, which collides Indo-Antarctica and Australo-Antarctica during the latest Mesoproterozoic and/or earliest Cambrian (Aitken et al., 2014; Boger, 2011). The rifting in the East Antarctica Rift System may have contributed to the rejuvenation of these regions from the Paleozoic to the Mesozoic (Ferraccioli et al., 2011). In Droning Maud Land, the Tonian Oceanic Arc Super Terrane (TOAST) is marked as a juvenile early Neoproterozoic province, separating Indo-Antarctic craton to the east (Jacobs et al., 2015; Ruppel et al., 2018). TOAST is thought to extend to a minimum of 800 km south inland until it reaches a region marked by a border negative magnetic anomaly (Ruppel et al., 2018).

West Antarctica is a younger region with two major rift systems, including the Jurassic Weddell Sea Rift (Jordan et al., 2013) and Cretaceous to Cenozoic West Antarctic Rift System (Jordan et al., 2020; Siddoway, 2008). The seismic model in this region shows a slow velocity structure which is impacted by hot and thin lithospheric mantle (An et al., 2015; Lloyd et al., 2020; Shen et al., 2018). With increased resolution, ANT-20 model also shows slow shear-wave speed anomalies along the Transantarctic Mountain front through the western Ross Ice Shelf, connecting with the Macquarie Triple Junction, which indicates a thermal effect of Cenozoic rifting (Lloyd et al., 2020).

3. Method

3.1. Modeling Concept

The seismic velocity and density structure of the mantle reflect variations in temperature, pressure, and composition (Stixrude & Lithgow-Bertelloni, 2005, 2011). In areas with high temperatures, seismic velocity drops dramatically, dominated by the attenuation effect. Thus, knowledge about the seismic attenuation model is a prerequisite to precisely modeling mantle thermal structure. However, the parameter in the seismic attenuation model is poorly defined, which requires extrapolating laboratory measurements to mantle conditions. In addition, when constructing a seismic velocity model, the choice of seismic attenuation model often varies by model (Lloyd et al., 2020).

Another important factor is mantle composition. Estimating temperature using seismic velocity alone, and so neglecting compositional variations can lead to significant errors where the assumed composition does not match the actual composition. Increasing velocities can be explained by either a colder lithosphere and/or a mantle that has undergone compositional changes due to depletion in partial melting events (Figure 2a). While both thermal and compositional changes can impact seismic velocity, they have different effects on the lithosphere's density structure. Therefore, variations in mantle density can serve as an additional constraint to differentiate the contributions of thermal and compositional effects (Kaban et al., 2014; Tesauro et al., 2014).

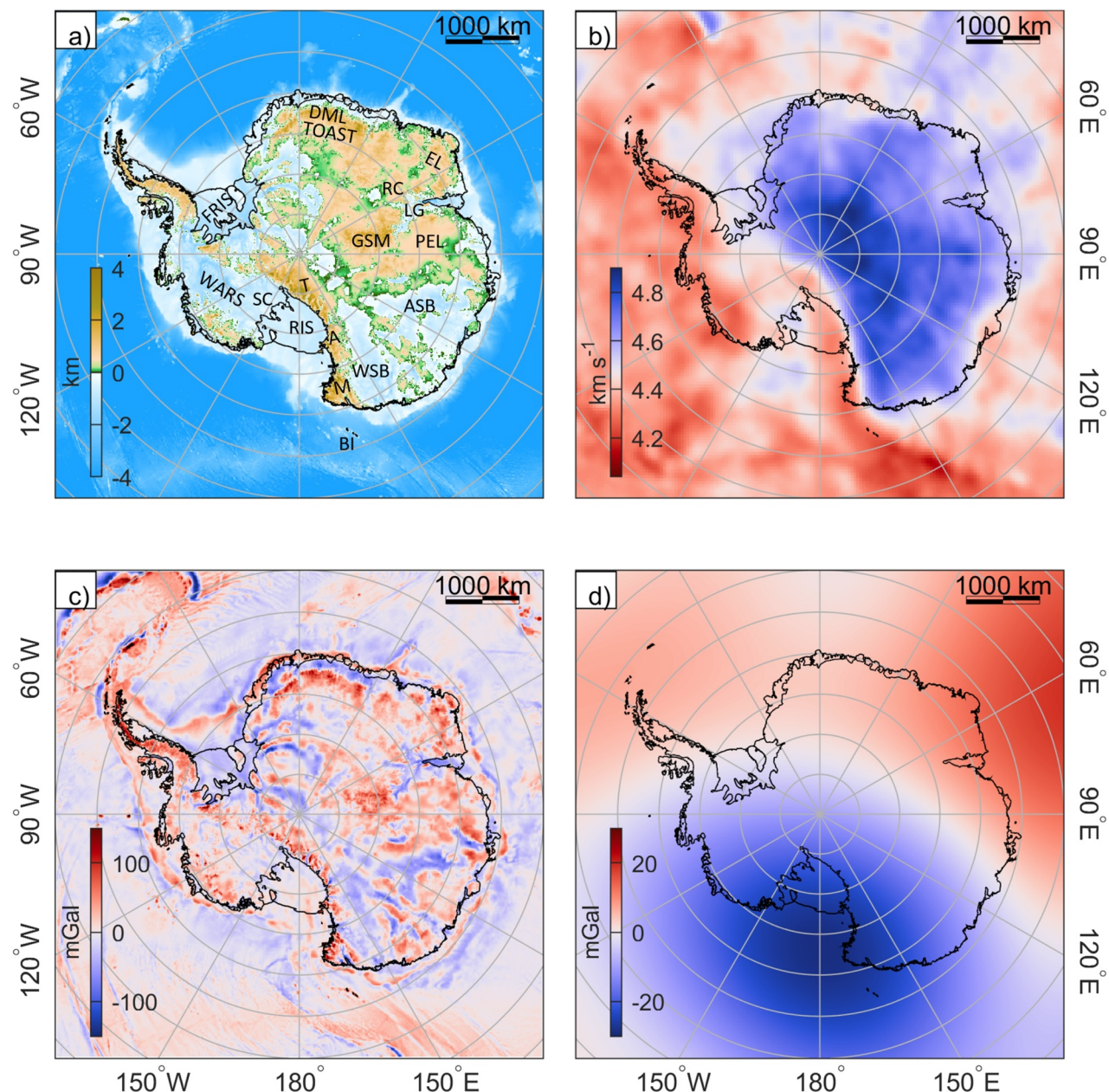


Figure 1. (a) Bedrock topography (Morlighem et al., 2020); (b) shear wave velocity (Lloyd et al., 2020) in Antarctica at 150 km depth. The white color shows the reference velocity speed (4.47 km s^{-1}) in the model STW105 (Kustowski et al., 2008); (c) combined airborne and satellite gravity model after removing the first 10 orders of the satellite gravity model GOCO06s (Kvas et al., 2019); (d) the first 10 orders of the satellite gravity model GOCO06s at 10 km ellipsoid height. Slow seismic velocity dominant in West Antarctica, while fast velocity is observed in East Antarctica (Kustowski et al., 2008). ASB, Aurora Subglacial Basin; BI, Balleny Islands; DML, Dronning Maud Land; EL, Enderby Land; FRIS, Filchner–Ronne Ice Shelf; GSM, Gamburtsev Subglacial Mountains; LG, Lambert Graben; PEL, Princess Elizabeth Land; RIS, Ross Ice Shelf; RC, Ruker Craton; SC, Siple Coase; TAM, Transantarctic Mountains; TOAST, Tonian Oceanic Arc Super Terrane; WARS, West Antarctic Rift System; WSB, Wilkes Subglacial Basin.

Using a locally derived temperature-pressure-seismic velocity constraint in Antarctica and the Southern Ocean (Hazzard et al., 2023), we estimated an optimized seismic velocity, temperature, and composition relationship. Applying this seismic velocity to temperature relationship, we converted seismic velocity into an initial mantle temperature and density, assuming a uniform initial composition (see Section 2.2). Gravity inversion was then used to resolve a correction to the density distribution so as to fit the gravity data. The final composition was selected based on the closest match between the density correction and synthetic density derived from various

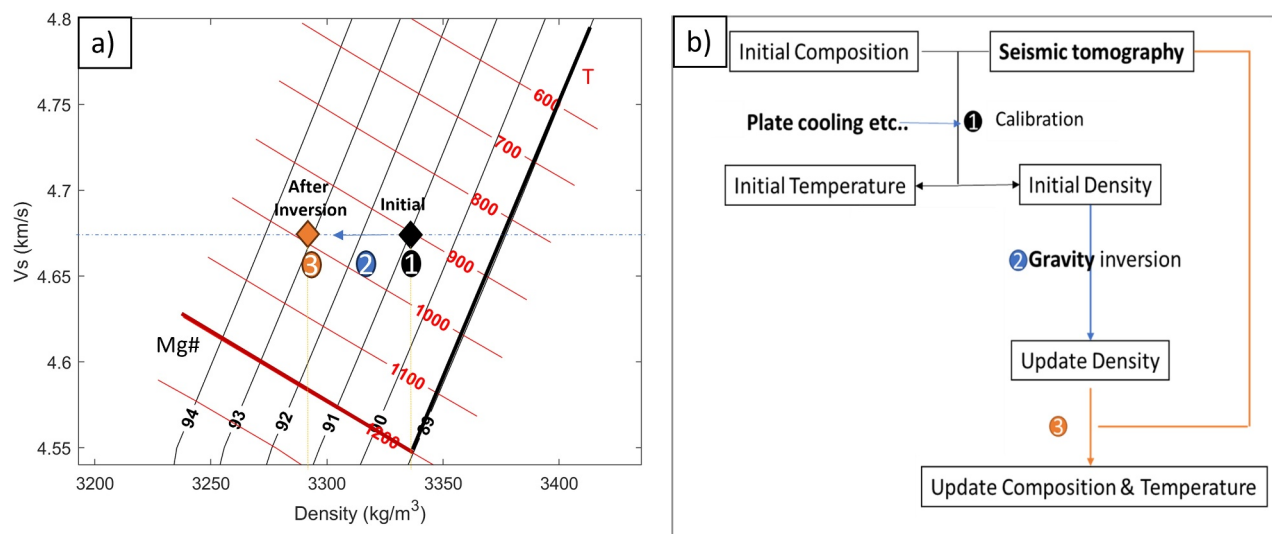


Figure 2. Modeling concept: seismic velocity and density vary with changing composition and temperature. (a) Variation in shear-wave velocity corresponding to changes in temperature and mantle composition; note the difference in resolved density changes. (b) Workflow for estimating composition, density, and temperature changes in Antarctica. Step 1: Estimate a Vs-temperature-density-composition relationship and generate an initial density and temperature field based on an initial mantle composition. Step 2: Use gravity inversion to resolve the mantle density distribution and update the density field. Step 3: Use the updated density field and seismic velocity to update the temperature and composition.

mantle compositions. From this self-consistent framework an updated temperature, composition, and density field model is derived that aligns with the seismic velocity model.

3.2. Calibrate Seismic Velocity to Density and Temperature Conversion

One of the key foundations for assessing thermal chemical properties using geophysical models is estimating the conversion of velocity to temperature and density. Priestley and McKenzie (2006) proposed an inversion framework to mitigate the mismatch between mineral physical parameters and seismic observations. The underlying philosophy is that mantle thermomechanical properties can be represented by well-constrained oceanic areas, allowing the use of a representative oceanic mantle composition to fit the relationship. However, petrological evidence suggests strong compositional heterogeneity within the oceanic and continental lithosphere (McDonough, 1990; Sun & McDonough, 1989). The lithospheric mantle undergoes melting, depletion associated with melt, and fertilization, leading to compositional variation. Therefore, it is crucial to consider compositional heterogeneity in the modeling framework.

Here we updated the conversion equation from (Hazzard et al., 2023; Richards et al., 2020) to include a term that accounts for changes in density and shear modulus due to mantle depletion and fertilization (Text S1 in Supporting Information S1). The posterior probability analysis from Hazzard et al. (2023) indicates that representing the temperature and velocity relationship with a uniform lithosphere and asthenosphere composition is not precise. The oceanic lithosphere requires variation in mantle composition to accurately represent areas with high seismic velocity in oceanic lithosphere. Additionally, a more fertile mantle composition is necessary to capture the adiabatic mantle temperature (Text S2 in Supporting Information S1). Thus, utilizing the same calibration data from Hazzard et al. (2023), we introduced distinct mantle compositions for the oceanic lithospheric mantle and the asthenosphere mantle. For the oceanic lithospheric mantle, we selected a lherzolite composition (Mg# 90.02, Maaløe and Aoki (1977)) to represent oceanic lithosphere after melt depletion. In contrast, for the adiabatic mantle, we employed an undepleted primitive mantle (PUM) composition (Mg# 89.27, McDonough and Sun (1995)). We adopted a linear variation model for mantle composition as our solution space (Kaban et al., 2014). In this model, the composition ranges between two endmembers: primitive mantle with an Mg# of 89.27 and depleted Archean mantle with an Mg# of 94. These compositions can be treated as peridotite consisting of four mineral phases (olivine, clinopyroxene, orthopyroxene, garnet) with an ideal solid solution of Mg and Fe end-member species in varying proportions (Kaban et al., 2014). Thus, the Mg# in our model represents the

degree of Fe-Mg exchange (for both Fe and Mg end-members) and the proportional variation of the four mineral phases (Text S2 in Supporting Information S1).

3.3. Gravity Inversion

We used the open-source python package esys-escript to solve the 3D gravity inversion problem (Gross et al., 2007, 2023; Schaa et al., 2016). In esys-escript, the gravity inversion problem is constructed as a linear partial differential equation. It uses the finite element method to discretize the model domain with an unstructured tetrahedral mesh. To solve the large scale gravity inversion in parallel, a novel integral preconditioned conjugate gradient method is used (Codd et al., 2021). During the inversion, we determine the density distribution of the whole lithosphere based on a reference model. We then minimize the total cost function based on the gravity misfit term J_d and the H1 regularization term $J_{(1)}$. The H1 regularization term is used to control the smoothness of the density correction. The total cost function J is defined.

$$J(m) = J_d + \mu_1 J_{(1)}(m)$$

With the factor μ_1 controlling the tradeoff between gravity misfit and the regularization term. $J_{(1)}$ denotes the H1-regularization term

$$J_{(1)}(m) = \frac{1}{2} \int \left(w_E \left(\frac{\partial m}{\partial E} \right)^2 + w_N \left(\frac{\partial m}{\partial N} \right)^2 + w_U \left(\frac{\partial m}{\partial U} \right)^2 \right) d_\Omega$$

where w_E , w_N and w_U are directional weighting factors in East, North and Up coordinates, respectively. Property functions m represents the target density correction term relative to initial density model. Ω is the computation domain.

In order to calculate gravity using ENU coordinates, we applied a transformation matrix to account for the changing direction of maximum gravity acceleration (Text S3 in Supporting Information S1). We used a partial differential equation to solve the gravity potential, then calculate the gravity potential gradient along the vertical direction.

We used the integral preconditioned conjugate gradient (I-PCG) solver (Codd et al., 2021). I-PCG can effectively precondition with the Hessian of the regularization term and avoid inverting a large sensitivity matrix. I-PCG with an unstructured mesh has similar accuracy to the Broyden–Fletcher–Goldfarb–Shanno (BFGS) solver on a structured mesh. The strong scalability of I-PCG ensures an efficient way to solve continental scale lithosphere structures using multi-cores. The detailed workflow for using I-PCG can be found in Codd et al. (2021).

The gravity response of an initial density model is removed from observation to form an initial data misfit (Aitken et al., 2015; Codd et al., 2021). The mean value of this initial data misfit is also removed. The cost function is then iteratively solved to generate the density correction relative to the initial model. The iteration is terminated when the gravity residual is sufficient small (12 mGal in the final model).

4. Model Setting

4.1. Domain Generation

We generated our gravity inversion domain using the unstructured tetrahedron mesh software Gmsh (Geuzaine & Remacle, 2009). An unstructured mesh was chosen due to its ability to adjust cell size to accommodate model resolution. The whole model domain includes the core gravity inversion domain, an air domain, and a coarse-resolution buffer zone (Codd et al., 2021). The core gravity inversion model domain extends to -45° South and 400 km depth with a 10 km resolution mesh. The extension of the core model domain covers the whole Antarctic continent and surrounding oceans. Its vertical extension is also in accordance with ANT-20, which includes the whole lithosphere and part of the asthenosphere mantle (Figure S2 in Supporting Information S1).

Due to the large extent of the model domain, we need to account for the curvature of the earth to fit the gravity. On a similar scale, previous continental-scale studies used geodetic coordinates including latitude, longitude, and height to construct the mesh (Aitken et al., 2015). However, geodetic coordinates with equiangular discretization

in the polar region led to small mesh at the pole and large mesh in the low latitude region. The geodetic coordinate also suffers from the singularity at the pole. We then seek to build our mesh domain at a local ENU (East, North and Up) Cartesian coordinate.

We built the initial 2D mesh domain at the polar stereographic coordinate system. The topography and Moho surface were deformed and re-projected into an ENU coordinate system to restore its actual shape with a curved 2D mesh. In this way, all topology and the shape of the Earth are preserved in our model domain. Finally, we built a 3D mesh with tetrahedrons based on the curved 2D mesh in the ENU coordinate system.

4.2. Gravity Data

The unstructured mesh enables us to include topography information in the model domain and to use free-air gravity data. The gravity data is a combination of continental scale near surface gravity compilation (AntGG, Scheinert et al. (2016)) with satellite gravity models (GOCO06s, Kvas et al. (2019)). As our model domain extends to 400 km depth, the lower order gravity components reflecting the deep mantle source were removed (Aitken et al., 2015). We subtracted the first 10 orders of the satellite gravity model at 10 km (Figure 1d).

4.3. Reference Model

Below the gravity observation layer, we included the bedrock topography from BedMachine Antarctica (Figures 1a, Morlighem et al., 2020). We used a mean value of topography in each 10 km by 10 km area to match the topography with gravity resolution. The total mass of water and ice from BedMachine was stored as a mass boundary condition at the topography surface to preserve the ice and water signal in the free-air gravity, avoiding the need to include these thin layers in the FEM mesh.

Constrained by the seismic Moho measurement and petrophysics data, Li and Aitken (2024) used an ensemble approach to generate a series of high-resolution crust models, including sedimentary basin thickness, crust density structure and Moho surface. These models fulfill the model constraints and highlight the lateral heterogeneity of the Antarctic crust. Here, we used the mean crustal structures of these model-ensembles as our initial crust structure. The output density value was interpolated into the mesh domain between the topography and Moho.

We used the shear-wave velocity model ANT-20 (Lloyd et al., 2020) to define our initial mantle structure. ANT-20 was constructed with 15 years of broadband seismic data recorded at 323 seismic stations across the whole continent. It has highlighted the small scale (horizontal <100 km) variability of mantle structures with a great improvement in resolution over prior global and previous continental scale models. While ANT-20 offers improved resolution, we acknowledge potential challenges, such as the effects of crustal thickness uncertainties on the mantle seismic velocities. These mixed signals can lead to discrepancies between seismic-derived mantle temperatures and conductive geotherms (Hazzard et al., 2023; Hoggard et al., 2020). The reliability of these features remains difficult to constrain due to the lack of detailed spatial uncertainty estimates for ANT-20. As a result, we do not explicitly account for seismic tomography uncertainties in our framework. Similar to Haeger et al. (2019), we treated seismic velocity as a ‘ground truth’ information to constrain mantle temperature and composition (Figure S16 in Supporting Information S1).

We converted the ANT-20 model mantle velocity into density and temperature. Although our method has the capacity to include different types of mantle composition during the conversion process, we converted the ANT-20 model based on a uniform composition of Mg# 91.3 (Figures S3 and S4 in Supporting Information S1). The reason for this is that the tectonic boundary for each domain is still poorly constrained. A predefined hard boundary might include incorrect constraints in the gravity inversion process. A uniform mantle with Mg# 91.3 is chosen due to its composition and density sitting in the middle zone between the upper and lower bounds of composition variation (PUM mantle and depleted mantle). We limited the density and composition changes that occur within the lithosphere. The asthenosphere is more uniform and less sensitive to composition change; thus, we used a uniform primitive mantle in the asthenosphere. Among all types of mantle compositions, a PUM composition (Mg# 89.27) has the lowest temperature based on the seismic velocity. Hence, we defined our initial lithosphere and asthenosphere boundaries based on a converted mantle temperature using PUM composition at the 1200°C isotherm. A 1200°C isotherm was chosen because it suggests a reasonable depth for continent-scale studies (Burgos et al., 2014; Richards et al., 2018).

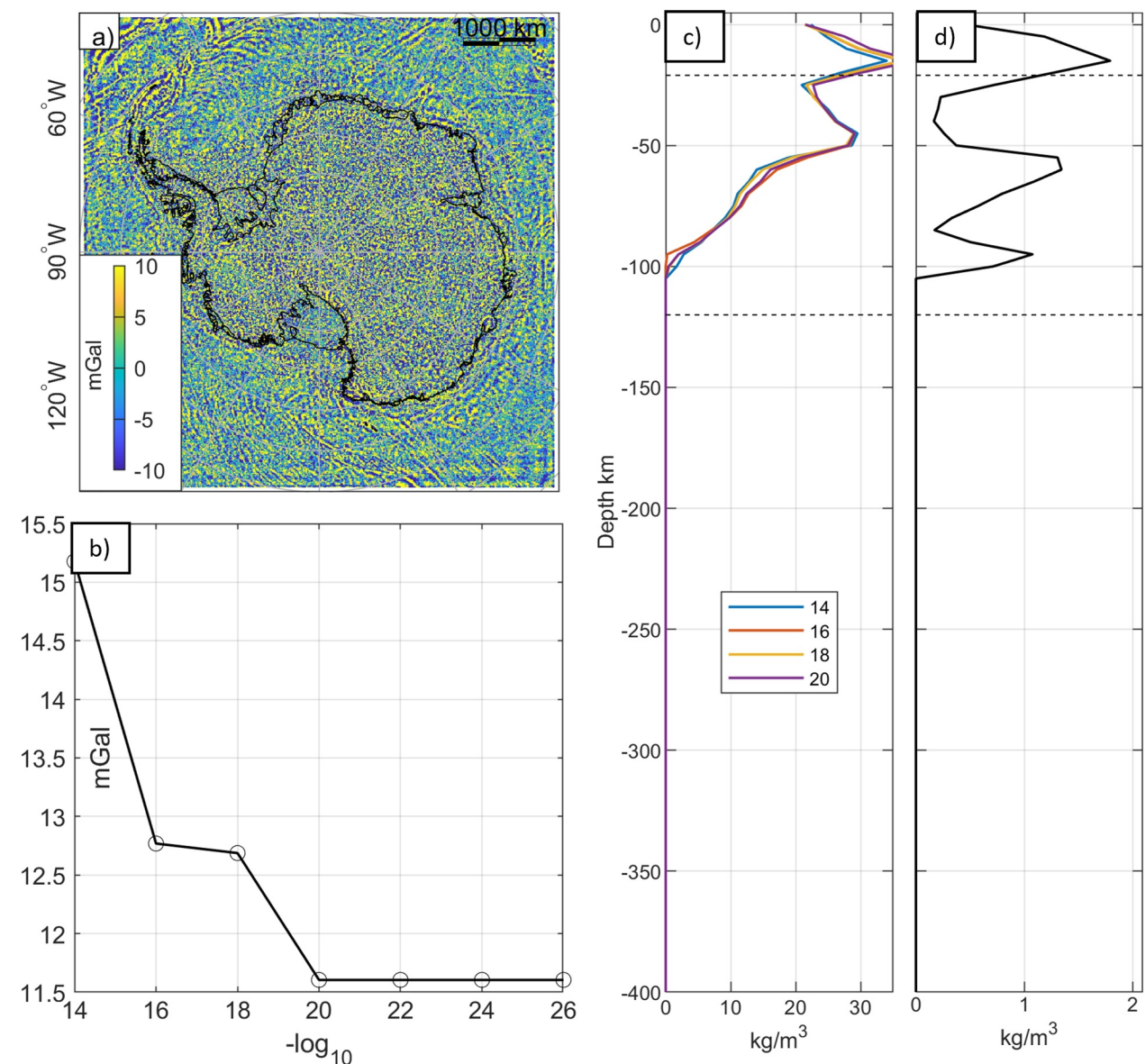


Figure 3. Model sensitivity and variability. (a) Gravity misfit with $\mu_1 = 10^{-20}$; (b) the RMS misfit change with regularization weight μ_1 ; (c) median value of the absolute value of density change in each depth bin for 4 μ_1 value. (d) median value of the standard deviation of cell to cell comparison for 4 different μ_1 models. The Dash line shows mean Moho and LAB depth.

5. Result

5.1. Model Variability and Sensitivity

Our gravity inversion algorithm solves the density distribution with a tradeoff between the data misfit and H1 regularization. We tested the weight of the H1 regularization term μ_1 ranging from 10^{-14} to 10^{-26} , with a decrement order of 10^{-2} . A decrease in μ_1 value causes a smoother model with a larger gravity misfit. We selected the μ_1 value based on two criteria. The first criterion was the upper bound of the final gravity misfit. The initial data misfit was 209 mGal. For any μ_1 resulting in a final misfit larger than 10% of the initial misfit, we treated it as insufficient to solve the gravity inversion problem, as the final misfit was higher than the data accuracy. The other criterion was the lower bound of the regularization parameter, where further reduction of weighting shows no significant improvement in data fitting. By reducing the regularization weighting, we see a decrease in the final data misfit (Figure 3b). Until it reaches a point (10^{-20}), we observe a stable data misfit (12 mGal). There are no

large-scale features in the final misfit map, which means the subsurface density structure is well resolved by the gravity inversion (Figure 3a). The remaining short wavelength misfit mainly reflects sharp topography information that cannot be resolved under the current mesh resolution. The misfit reduction limitation is generally controlled by the mesh size in particular how topography is represented in the mesh (Codd et al., 2021).

The variability of the four selected models is shown in Figure 3c. Here, we plot the median for absolute density correction with depth and cell-to-cell density variability for all four selected models. We see a similar density pattern with different regularization terms. The amplitude of the density correction decreases with an increase in depth. The major change is located in the crust and uppermost mantle. A lower regularization weight generates a localized shallow density structure to reduce the data misfit further. In all these cases, the density variations follow a smooth depth-dependent relationship characterized by increasing variability at mid-to-lower crustal depths and decreasing variability within the deeper mantle. The vertical dipping and extension of the resolved density structure tend to be similar regarding choosing the regularization term.

We selected 10^{-20} as the regularization term for the final model. Under this regularization, the model possesses a low data misfit. Further reduction in regularization weighting shows no major improvement in fitting gravity.

Gravity inversion has low depth sensitivity. In this continental-scale application, the depth sensitivity is controlled by the vertical extension of the gravity inversion domain and the gravity kernel. The total model domain includes a horizontal extension of $6,600 \times 6,600$ km and a vertical extension of 400 km. With an average LAB change of 100–250 km in West and East Antarctica, the overall depth sensitivity varies in each domain.

It is worth mentioning that the smooth regularization constraint only applies to the correction term, not the reference density model. Therefore, any sharp features in the starting model are likely to be present in the final model unless they generate a large gravity misfit. This ensures we preserve boundaries between transition areas in each model domain. The resolved density correction tends to concentrate in the top half of the gravity inversion domain. The density in the upper lithospheric mantle changes within a range of ± 60 kg/m³. Within this range, the vertical density variation provides a good constraint for the compositional changes in the upper mantle.

5.2. Density Distribution

Gravity inversion solves the gravity misfit, which re-distributes the density distribution in the lithosphere. The majority of density correction terms are within ± 60 kg/m³, with a median absolute value of less than 12 kg/m³. The thin West Antarctic lithosphere leads to a narrow gravity inversion space causing localized higher density values. The negative density correction mainly occurs in East Antarctica, which corrects for compositional effects and temperature accounting for the fast seismic velocity field. Density correction in West Antarctica is generally positive but with localized negative density corrections. The overall trend leads to a more depleted type mantle in East Antarctica and a more primitive mantle in West Antarctica, which fits the current understanding of continent based surface geology and geophysical data (Boger, 2011; Jordan et al., 2020).

Combining the density correction with the initial density field, we show the total density distribution of the Antarctic lithosphere (Figure 4). The initial density is shown in Figure S3. In the lithosphere, we see an overall similar density distribution to the initial density distribution but with systematic changes. In East Antarctica, the original dense lithosphere is modified by the gravity inversion, indicating that fast seismic velocities in this region require a compositional adjustment. Below the Moho, around 100–150 km, East Antarctica is characterized by a higher density compared with West Antarctica. This is attributed to the combined effects of lower temperatures (increase density) with a more depleted mantle composition (decrease density). With a greater depth (200–300 km), the density distribution is reversed, as the dense asthenosphere in West Antarctica contrasts with the less dense lithosphere mantle in East Antarctica. Within the asthenosphere, the density in East Antarctica remains higher than in West Antarctica, primarily driven by the lower temperatures of the East Antarctic asthenospheric mantle (Figures 4c, 4d and 5c, 5d).

5.3. Temperature Distribution

The initial temperature distribution closely reflects the input seismic velocity models, as temperature increases with a decrease in seismic velocity. Here we show the representative depth slices for 100, 150, 200, and 250 km in Figure 5. Clearly, the dominant difference is the cold East Antarctica lithosphere contrasted with the hot West Antarctica lithosphere. At 100 km depth, East Antarctica is around 800°C, while West Antarctica is over 1,100°C,

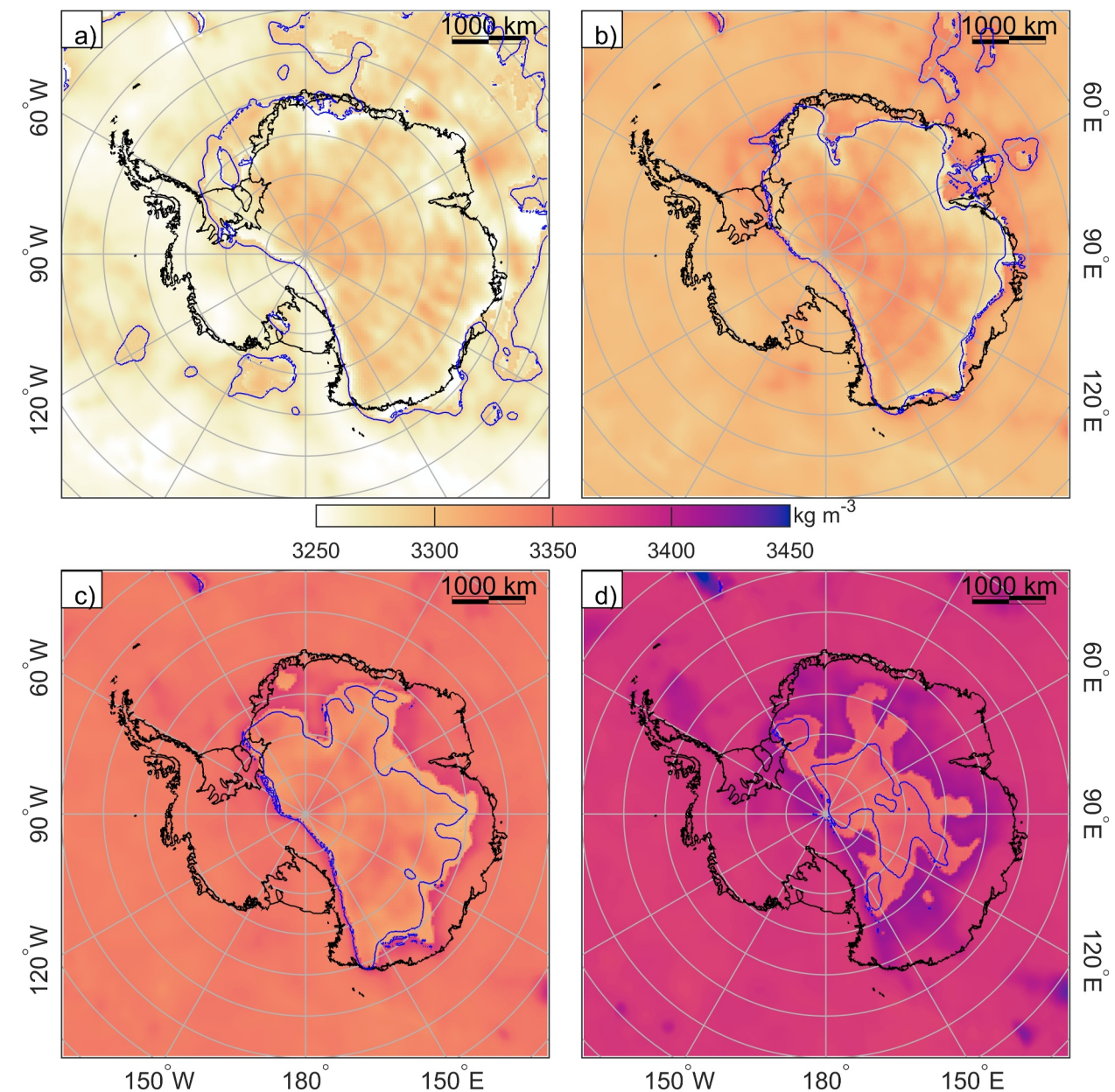


Figure 4. Depth slice of the final density distribution at (a) 100 km, (b) 150 km, (c) 200 km, and (d) 250 km. The blue line marks the updated LAB ($1,200^{\circ}\text{C}$ isotherm; see Section 5.2).

with a local temperature higher than $1,300^{\circ}\text{C}$. This pattern shows major West Antarctica is in the asthenosphere at this depth, while the cratonic-type lithosphere in East Antarctica is still cold. Local anomalies, including the center of East Antarctica and the Princess Elizabeth Land region, are even colder, with temperatures less than 400°C . At 150 km depth, the coastal region in East Antarctica, including Wilkes Land, Wilkes Subglacial Basin, and Dronning Maud Land, shows higher temperatures, which are already in the asthenosphere zone. In West Antarctica, the predominant feature is the connection of the Transantarctic Mountains through the western front of Ross Ice Shelf into Balleny Islands, and the elevated hot mantle in Marie Byrd Land is connected to the offshore region. These features extend to at least 250 km of depth; this pattern suggests a deeper heat source for these anomalies.

Compared with the initial temperature model, our result remains a similar pattern, but with changes in the local areas. Considering compositional change, the resolved temperature is up to 200°C higher than the initial

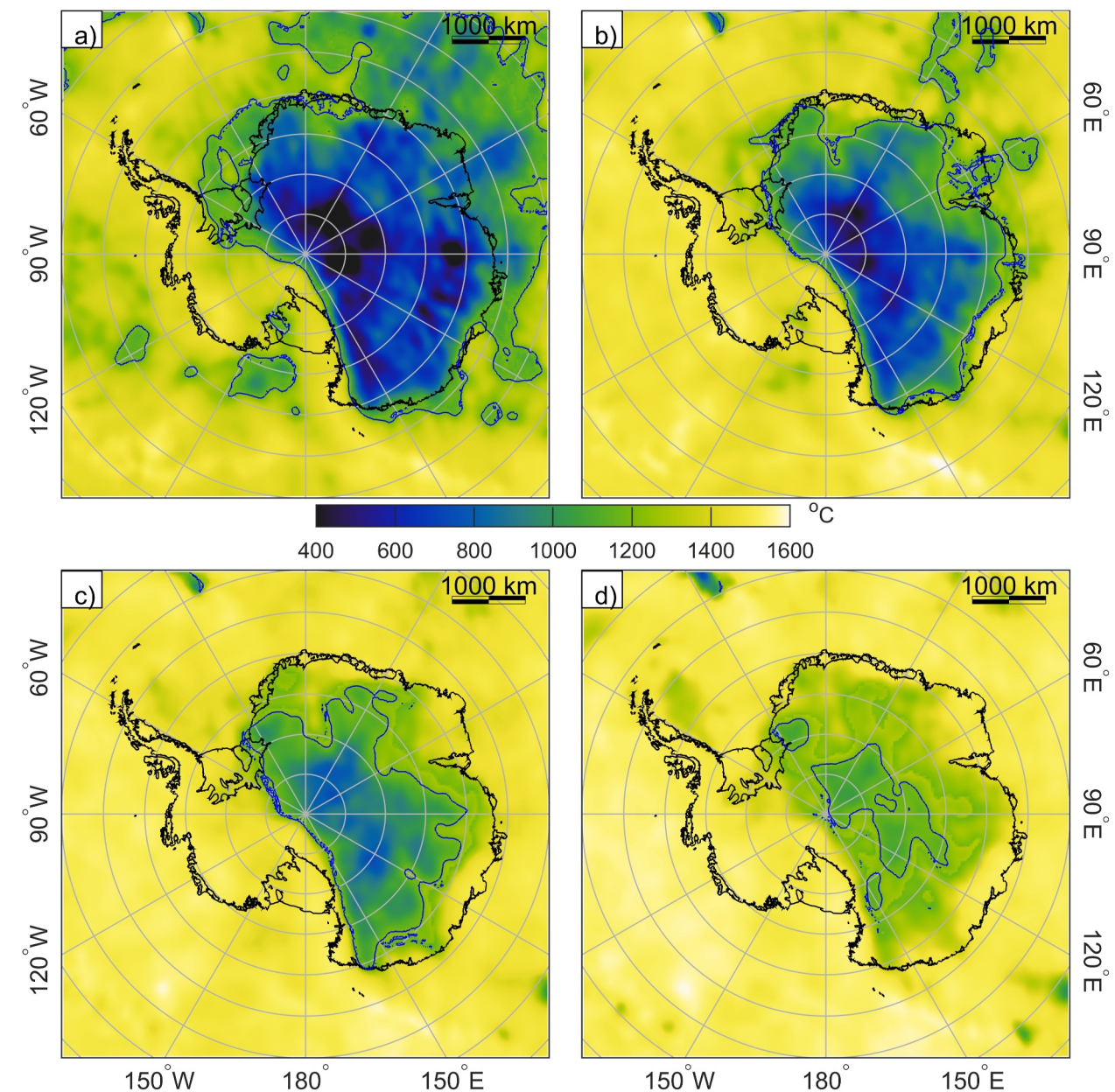


Figure 5. Temperature depth slice at (a) 100 km; (b) 150 km; (c) 200 km; (d) 250 km after the gravity inversion. The blue line marks the updated LAB ($1,200^{\circ}\text{C}$) isotherm; see Section 5.2.

temperature due to accounting for mantle depletion (Figure S5 in Supporting Information S1). Although the depletion leads to a higher estimated temperature in East Antarctica, the low temperature anomaly remains in central East Antarctica and Princess Elizabeth Land. The major change happens in the Dronning Maud Land region and Wilkes Land near the grounding line, where the compositional variation leads to higher temperatures distinguished from surrounding areas.

5.4. Composition Distribution

Based on the density correction result, we also updated changes in composition in terms of Mg#. The depletion variations with representative depth slices are shown in Figure 6. The compositional variation largely occurred in East Antarctica, with major areas showing Mg# higher than 91.3, which indicates a depleted lithospheric mantle.

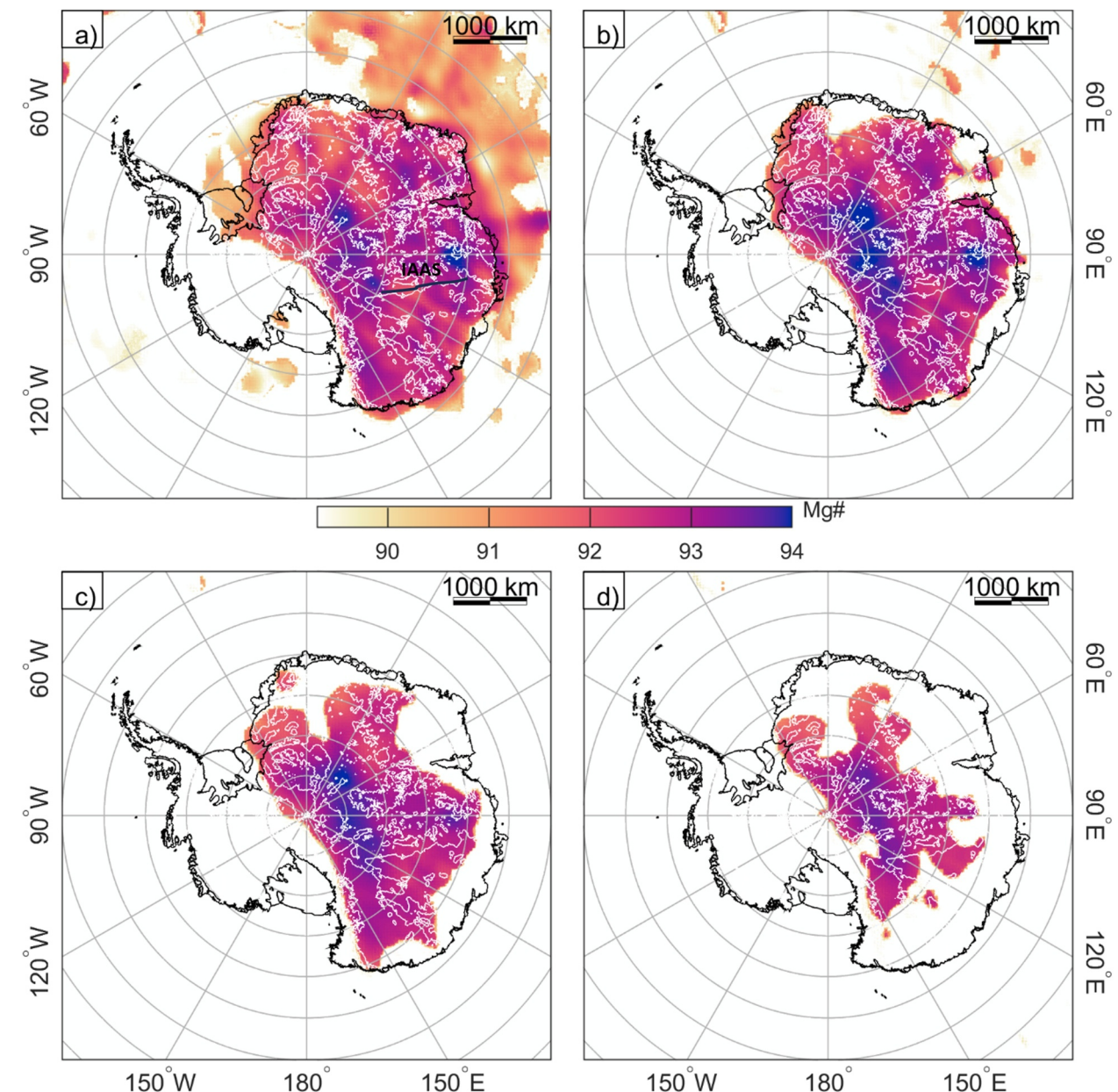


Figure 6. Compositional change Mg# with depth slice at (a) 100 km; (b) 150 km; (c) 200 km; (d) 250 km after the inversion. The bedrock topography is shown in white contour for reference. Depleted mantle composition is required to match velocity and density model in East Antarctica. West Antarctica shows primitive mantle. IAAS, Indo-Australo-Antarctic Suture.

The highly depleted lithosphere ($\text{Mg}\# > 93$) is shown at Princess Elizabeth Land and the center of East Antarctica, extending to the south portion of the Gamburtsev Subglacial Mountains.

Coastal region shows lower Mg#. Areas including the Lambert Graben and Enderby Land exhibit relatively low depletion. The Lambert Graben shows lower Mg# compare with surrounding Gamburtsev Subglacial Mountains and Ruker Craton in Enderby Land. This area might have been reactivated during the formation of Gondwana (Ferraccioli et al., 2011; Lisker et al., 2003). Our result generally shows a less depleted mantle in Australo-Antarctica sector separate from high depletion in Indo-Antarctica by the Indo-Australo-Antarctic Suture (Aitken et al., 2014). The area with less depleted mantle also shows large sedimentary basins, in contrast to areas with more depleted mantle, which have a predominant basement structure. This suggests that the plate tectonics has a profound impact on sedimentary basin formation in East Antarctica (Aitken et al., 2023).

A large area of central Dronning Maud Land shows a less depleted mantle. In this region, the TOAST is suggested to be formed by juvenile early Mesoproterozoic to Neoproterozoic terranes (Jacobs et al., 2015; Ruppel et al., 2018). Our model suggests that low Mg# supports the early Neoproterozoic to Phanerozoic to age of this region. The low Mg# region extends to 80°S, which might mark to southern extension of TOAST.

The resolved Mg# value in our model is higher than previous model estimations using geophysics data (e.g., max Mg# = 92 in Haeger et al. (2019)). The highest Mg# = 94 is also higher than the global average Archean lithosphere composition record in the mantle xenolith, but within the range reported by literature (e.g., Mg# of olivine range from 88 to 94 in Gaul et al. (2000)).

Our resolved high Mg# value could be explained by the choice of the initial lithospheric mantle composition. Here, we ran an additional inversion with a PUM lithospheric mantle as the starting mantle composition, following the approach of Haeger et al. (2019). In this case, we observed a lower Mg# number compared to the model starting with a lithospheric mantle having Mg# = 91.3 (see Figure S10 in Supporting Information S1). However, this model is not able to accommodate the resolved positive density change in West Antarctica. Instead, starting in the middle of the solution space is necessary to accommodate the density changes in both East and West Antarctica. Therefore, we prefer the model with a higher Mg# in East Antarctica as it provides a better model fit.

We should point out, the Mg# should not simply be treated as an indicator of geological age (unless it lies at the endmember of the Mg#) but rather as a reflection of the degree of mantle depletion. In addition, in our framework, Mg# is a simplified term representing both mantle depletion and mineral fractions (Kaban et al., 2014). The variation of Mg# is used to explain the density variation observed from gravity inversion. However, other minerals (e.g., spinel and chromium) could also complicate the mantle density and the relationship between shear-wave velocity and temperature (Kaban et al., 2014).

6. Discussion

6.1. Model Uncertainties

In our study, we utilized a two-layer upper mantle composition model to calibrate variations in shear modulus and density due to changes in temperature, pressure, and composition. Although this calibration process captures large-scale mantle variations, it's important to acknowledge the uncertainties that need to be considered to fully account for the thermodynamic processes in the mantle.

Given the lack of precise observations of mantle composition, we use a spinel lherzolitic oceanic lithosphere composition (Mg# 90.02) and a primitive asthenosphere mantle (Mg# 89.27) for calibration. This composition, derived from the global average of spinel lherzolite xenoliths (Mg# 90.02, Maaløe and Aoki (1977)), fits well with data constraints and aligns with parameterization for constructing a plate cooling model using decompression melting of dry aluminous lherzolite (Katz et al., 2003; Shortle et al., 2014). However, evidence from mid-ocean ridges surrounding the Antarctic continent suggests a highly variable mantle potential temperature (Dalton et al., 2014), possibly indicating a spatial variable melt fraction with heterogeneous mantle composition. Thus, a compositional constraint in the continental lithosphere is required to further refine the temperature–shear wave velocity relationship. For example, paleogeotherms derived from mantle xenolith could be a useful constraint (Hoggard et al., 2020); however, their availability in Antarctica is limited (Martin, 2023).

Our parameterization is simplistic in assuming that the bulk shear modulus and density vary linearly with mantle mineral fractions and chemical changes, reflecting mantle depletion (Mg#). We recognize that the thermodynamic process is more complex than this framework assumes, where factors such as water variation and partial melt also contribute to shear wave velocity changes (Karato & Jung, 1998). In addition, the presence of other minerals could cause the non-linear behavior of density and seismic velocity to the mantle composition. For example, the inclusion of Al in garnet significantly influences the formation of high-density, high-V_s phases, thus changing how V_s varies due to composition change (Afonso & Schutt, 2012). In addition, processes including metasomatic alternation, mantle fertilization due to basaltic melt would further complicate this relationship.

We would like to point out that a simplistic parameterization is necessary to quantify the contributions of thermal and compositional variations to mantle seismic velocity, as the calibration process is inherently underdetermined. However, our simplistic parameterization introduces apparent uncertainties. We identify and discuss four primary uncertainties in interpreting our model: (a) the sensitivity of V_s to melt fraction, (b) the trade-off between thermal

and compositional structures in our parameterization, (c) the impact of crustal density on resolved mantle properties, (d) the impact of uncertainties in seismic tomography model.

Shear modulus variations with mantle composition strongly govern how compositional changes affect seismic velocity in our model. While there are different views on the role of composition, recent experimental data suggest a maximum 2% increase in V_s due to melt depletion (Afonso & Schutt, 2012; Schutt & Lesher, 2006). Our parameterization, based on Kaban et al. (2014) and Haeger et al. (2019), supports this conclusion, indicating that considering mantle composition can refine resolved temperatures by up to 200°C, but thermal effects act as the primary control on V_s .

A simple example can be made by following the 900°C isotherm at 100 km depth (Figure 2a), a change in mantle composition from Mg# 89 to 94 increases V_s from 4.65 km/s to 4.72 km/s, representing a 1.5% velocity change. This is consistent with the maximum of 2% V_s increase due to melt depletion by experimental data. Expanding the Mg# space or using a larger value for shear modulus varies with composition could exaggerate the compositional effect, but this would deviate from experimental findings and observations from natural xenolith samples.

As some parameters exhibit strong trade-offs with each other (Figure S11 in Supporting Information S1), there is potential for a trade-off between the modeled thermal and compositional structures. Among these, two key parameters—shear modulus sensitivity to temperature and composition—primarily control the resolved temperature and compositional structure.

A sensitivity test (Text S2 in Supporting Information S1) demonstrates that the impact of variations in these internal parameters on the trade-off between temperature and composition is minimal. The resulting uncertainties are less than 20°C for temperature and 0.2 for composition, highlighting the robustness of our framework despite the presence of parameter trade-offs.

The resolved mantle density structure has a direct influence on the modeled thermal and compositional structure, and it is strongly linked to the initial crustal density model (Haeger et al., 2019). To assess the impact of crustal structure on the resolved mantle properties, we conducted additional sensitivity tests (Text S4 in Supporting Information S1).

We perturbed the initial crustal structure within the range defined by the model ensemble from Li and Aitken (2024) and reran the gravity inversion to compute new temperature and composition distributions. The results showed that changes in the crustal density caused small-scale change in the gravity misfit, which, in turn, led to variations in the resolved mantle thermal and compositional structures. Despite these changes, the overarching patterns remained consistent. Resolved temperature variations due to crustal density changes were within ±20°C, and Mg# variations were less than 0.4 (Text S4 in Supporting Information S1).

We acknowledge that our framework does not account for uncertainties inherent in seismic tomography models. These models are influenced by factors such as input data, initial model assumptions, and regularization choices, which fall outside the constraints of our workflow. Given that a 1% change in seismic velocity can result in temperature variations exceeding 100°C, the uncertainties associated with the first three aspects—sensitivity of V_s to melt fraction, trade-offs between thermal and compositional structures, and the impact of crustal density on resolved mantle properties—remain small in comparison to the uncertainties inherent in the seismic tomography model (Text S4 in Supporting Information S1). In the case that input seismic constraints significantly deviate from the true structure, gravity data has limited power to correct these inaccuracies.

Despite these limitations and uncertainties, our work offers a self-consistent framework for quantifying the thermal and compositional structure of the Antarctic mantle. A qualitative representation of mantle conditions may be achieved by combining the resolved thermal and compositional characteristics. For example, fertile mantle and metasomatically altered regions may exhibit similar seismic signatures but have different density signature. In addition, a fertile mantle and a “refertilized” mantle might display similar densities but can differ in seismic velocity signatures. This underscores the importance of integrating multiple geophysical datasets to better constrain mantle conditions.

However, caution should be made when attempting to make a quantitative interpretation of mantle conditions (e.g., percentage of melt extraction, metasomatism), as the current resolution of seismic tomography models and the nonlinear nature of thermal dynamics present challenges in fully resolving mantle conditions quantitatively.

Nevertheless, there is potential for incorporating other geophysical data, such as magnetotellurics (MT), to account for these complex mantle conditions (Manassero et al., 2024; Ramirez et al., 2022).

We highlight the complex nature to resolve mantle thermal and composition conditions. Despite these challenges, our results show that by considering compositional heterogeneity, the resolved lithospheric mantle temperature can vary significantly. Utilizing this newly resolved mantle thermal structure, we explore how a warmer East Antarctica lithospheric mantle aids in determining lithosphere thickness, geothermal heat flow, and mantle viscosity, and its implication of the stability of East Antarctic Ice sheet.

6.2. Implication for Lithosphere Thickness

From the updated 3D temperature field, we calculate the thermal LAB based on the 1,200°C isotherm (Burgos et al., 2014; Hazzard et al., 2023; Richards et al., 2018). The resolved LAB shows a predominant difference between East Antarctica and West Antarctica. In West Antarctica, the LAB ranges from 60 to 100 km. In a few regions, the lithosphere is thinner than 80 km, such as Marie Byrd Land and the Ross Sea front of the Transantarctic Mountains. The extension of the thin lithosphere starts from the western flank of Victoria Land and, through TAM, extends to the Ronne Ice Shelf. Interestingly, the adjacent Filchner Ice Shelf shows a thicker lithosphere. The LAB in East Antarctica is deeper, with an average depth of over 250 km and large spatial heterogeneity. The central East Antarctica shows an extremely deep LAB, with a depth of over 360 km. LAB at the coast region is generally shallower; Wilkes Land and Dronning Maud Land have LAB of less than 150 km.

When comparing the updated 3D temperature field with the uniform PUM mantle, we observe that mantle depletion can lead to estimated temperature differences of up to 200°C. When this temperature change is factored in, the LAB becomes thinner in localized areas. According to our updated thermal model, the LAB could be up to 150 km thinner than a uniform PUM composition, as illustrated in Figure 7b. We also note that the resolved LAB exceeds the uncertainty range of the model resolved using the Bayesian framework, which only considers the variability of all thermomechanical properties with a consistent composition (Hazzard et al., 2023). This observation leads us to suggest that it is necessary to take compositional variation into account when determining the thickness of the continental lithosphere from seismic velocity.

We noticed that the resolved LAB is anomalously thick in East Antarctica near the Recovery Glacier region. A similarly thick LAB is also suggested by Hazzard et al. (2023) using the same seismic tomography model (ANT-20). However, this thick LAB is not resolved using other seismic tomography models (Hazzard et al., 2023). The nature of this anomalously thick LAB is difficult to constrain, but it appears to be an inherent structure indicated by ANT-20. We also observed that the seismic station coverage in this region is sparse; therefore, a denser seismic deployment in the future could help constrain the reliability of this anomalously thick LAB.

6.3. Implications for Geothermal Heat Flow

In addition to estimating the LAB from the 3D temperature field, we use the resolved mantle temperature to estimate a steady-state geotherm. We focus on how the resolved mantle thermal structure impacts GHF. Here, we adapt the method outlined by McKenzie et al. (2005) to fit a steady-state heat flow to match the resolved mantle thermal profile and LAB. The steady-state heat flow was chosen to reduce the potential impact of crustal structure signals bleeding into the mantle, which could result in anomalously high temperatures (Figure S16 in Supporting Information S1). The thermal parameters, including thermal conductivity and radiogenic heat production in the crust, are constant and their variation is not constrained in our model. We use a constant crust thermal conductivity of $2.5 \text{ W m}^{-1} \text{ K}^{-1}$, radiogenic heat production for the upper crust of $1 \mu\text{W/m}^3$, and $0.3 \mu\text{W/m}^3$ in the lower crust (Hazzard et al., 2023).

Our estimation of GHF averages 76 mW/m^2 in West Antarctica and 40 mW/m^2 in East Antarctica. Our new heat flow map shows large parts of West Antarctica have heat flow larger than 70 mW/m^2 , with local hot spots at Amundsen Sea Embayment, Marie Byrd Land, and south of the Ross Ice Shelf. This estimation is in a similar range with previous continental scale estimations based on seismic tomography (An et al., 2015; Shen et al., 2020), magnetic (Martos et al., 2017), and statistical methods (Lösing & Ebbing, 2021; Stål et al., 2021), but our model is not able to resolve high GHF at the upper stream of Pine Island Glacier ($>90 \text{ mW/m}^2$), as derived by satellite magnetic data (Purucker, 2013) (Figure S9 in Supporting Information S1).

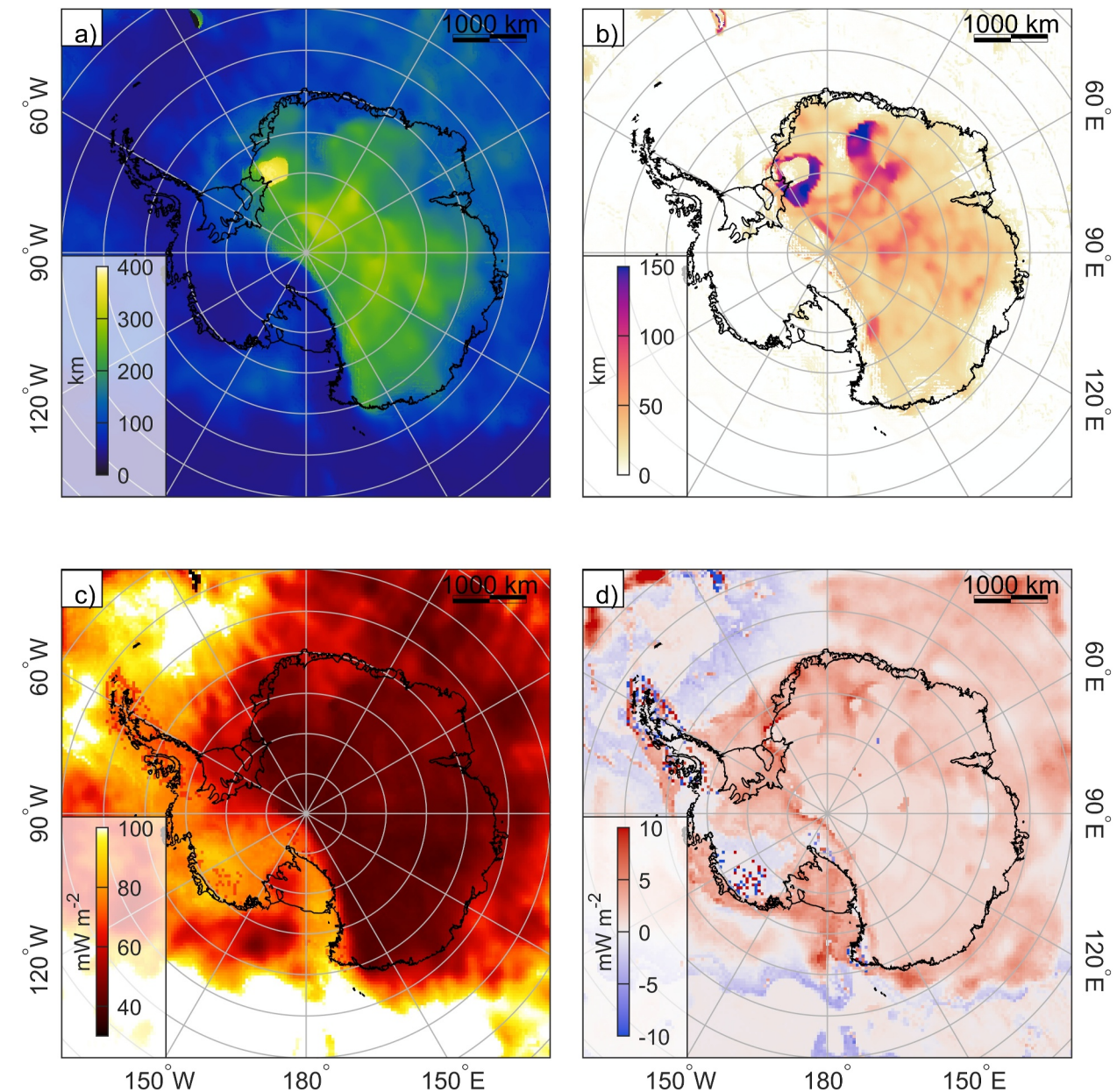


Figure 7. Implications of considering mantle composition variation for LAB and GHF. (a) LAB from the updated temperature model; (b) LAB difference between using the updated temperature and the initial temperature using PUM composition (c) GHF from the updated mantle temperature field; (d) GHF difference between using the updated temperature and the initial temperate using PUM composition. The updated temperate model indicates a thinner LAB and higher GHF. The black outline in (d) show ice drainage basin boundaries (Rignot et al., 2019).

Due to the fact that, we do not consider the variation of crust heat production contribution to the GHF (Hazzard & Richards, 2024; Li & Aitken, 2024), our resolved GHF is not able to reproduce the extreme high GHF ($> 100 \text{ mW/m}^2$) estimated based on radar echo strength (Schroeder et al., 2014) and magnetic data (Dziadek et al., 2021) beneath Thwaites Glacier. In addition, these high GHF values are potentially linked with the basal hydrological processes (Gooch et al., 2016; Li et al., 2022), which cannot be resolve using only the mantle temperature field. Nonetheless, our result highlights a significant mantle contribution to surface heat flow in West Antarctica linked to the shallow LAB in the region.

In East Antarctica, we observe locally elevated GHF compared to estimates that do not factor in compositional variations. In areas resolved with a depleted mantle composition, earlier estimates underestimate heat flow by

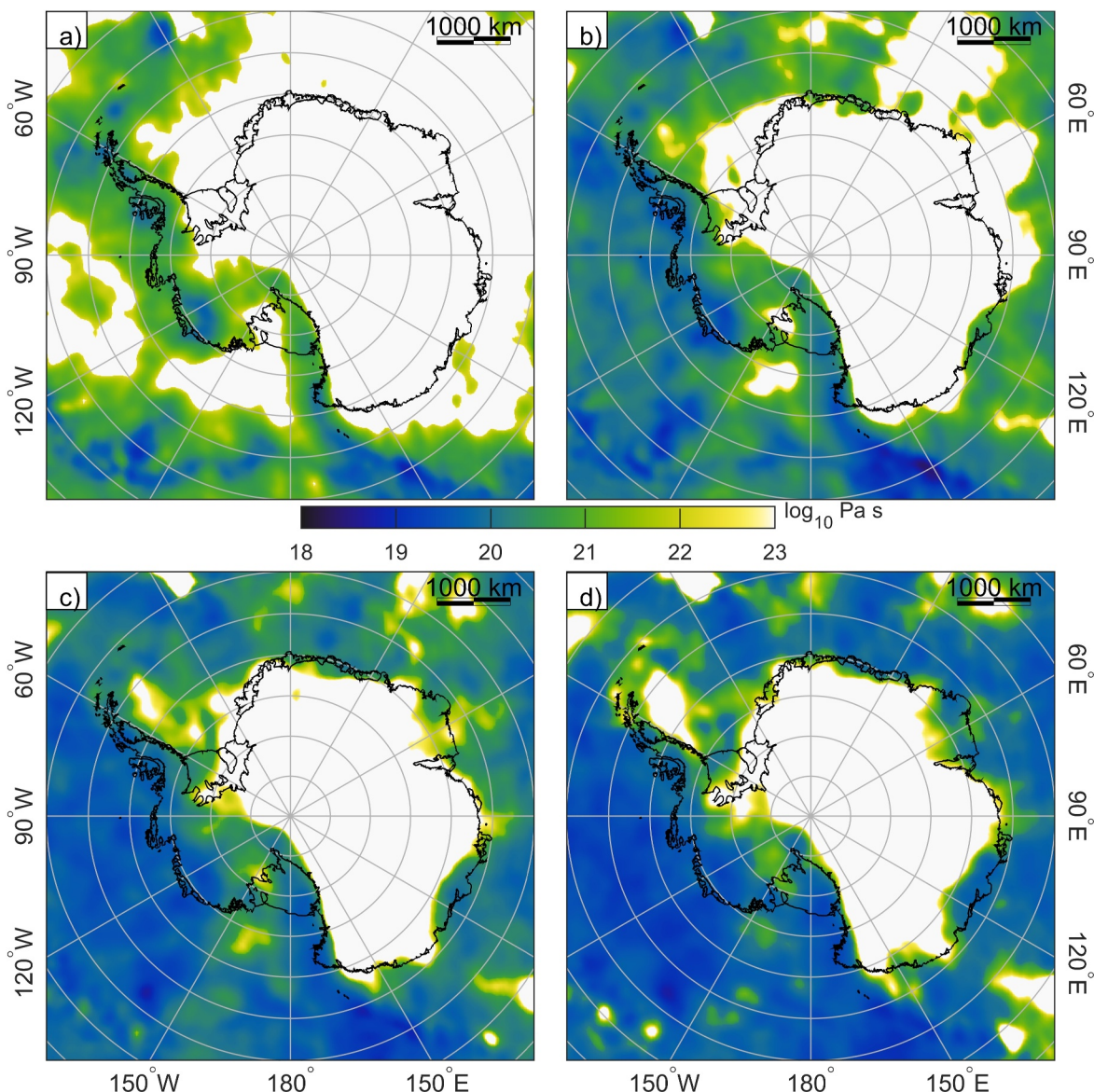


Figure 8. Depth slice for mantle viscosity at (a) 100 km, (b) 150 km, (c) 200 km, (d) 250 km depth. The mantle viscosity is calculated based on the updated temperature field. The upper limit is set at 10^{23} Pa s. Areas with a viscosity higher than 10^{23} Pa s predominate in elastic response.

approximately $3\text{--}10 \text{ mW/m}^2$. These findings highlight the significance of compositional heterogeneity when assessing mantle heat flow anomalies in future estimations of geothermal heat flow. Although GHF relevant to ice sheet dynamics operates on a smaller scale (McCormack et al., 2022), accurately representing GHF contribution from the mantle is a prerequisite to fully resolving the GHF and understanding its contribution to ice sheet instability.

6.4. Implication for Mantle Viscosity

Based on the newly defined temperature structure, we calculate diffusion creep viscosity based on the temperature anomaly related to the solid state. The viscosity estimation is shown in Figure 8. At 100 km depth, a sharp boundary follows the Victoria Land through the Transantarctic Mountains divide, which divides the high viscosity East Antarctica lithosphere with the relatively low-viscosity asthenosphere mantle in West Antarctica. Within large region in West Antarctica, viscosity varies within the range $10^{19}\text{--}23$ Pa s. The lowest viscosity (5×10^{19} Pa s) is shown in Marie Byrd Land. A major region in East Antarctica shows viscosity $>10^{23}$ Pa s with

an elastic response. With the increase in depth, the viscosity is generally constant within West Antarctica. From 200 km depth, the coastal region in Enderly Land, Wilkes Land, shows a relative low viscosity of 6×10^{19} – 10^{20} Pa s.

Our viscosity estimation generally has a similar pattern but with a higher value than that based on GNSS estimation. In the Amundsen Sea Embayment, GPS estimation suggests near 4×10^{18} Pa for the first 200 km mantle (Barletta et al., 2018). Our estimation is higher with a viscosity around 8×10^{19} – 10^{20} Pa s. The high viscosity on the Siple coast is also captured by our model, where it has a viscosity of 2×10^{20} – 10^{21} Pa s (Nield et al., 2016). The Filchner–Ronne Ice Shelf also has a higher viscosity compare with the Siple Coast. The extremely low viscosity in the Antarctic Peninsula (10^{18} Pa s, Nield et al. (2014)) is not resolved by our estimation. The viscosity of the Antarctic Peninsula shows (7×10^{19} – 10^{20} Pa s) in our model.

The reason for this discrepancy can be related to using different ice loading timescales in a steady-state (our seismic-inferred) estimation and time-dependent (geodetic) apparent viscosity (see Hazzard et al. (2023)). For a geodetic viscosity estimation, using a short ice loading history led to the activated deformation focused on the shallow upper mantle, and it was expected to see a lower mantle viscosity compared with the estimation using a longer ice loading history. Hazzard et al. (2023) showed that the low mantle viscosity estimated by geodetic estimation can be reproduced by calculating a time-dependent viscosity using seismically informed parameters with a short ice loading history.

In addition to comparing with the geodetic observation, we also compare the resolved mantle viscosity with and without considering mantle composition variation. Although our model predicts higher mantle temperatures compared to a model with uniform composition, we find that the estimated mantle viscosity is not necessarily low enough to impact ice sheet stability in the near term. An area with a large temperature change is located further inland, where the mantle viscosity is high ($>10^{23}$ Pa). The relaxation times of a Maxwell fluid can be approximated by dividing viscosity by shear modulus ($\sim 7.5 \times 10^{10}$ Pa in our model), thus a higher viscosity ($>10^{23}$ Pa) has a millennial timescale relaxation time (>40 k years). Even when the composition variation is factored into the estimated temperature, the increase in the estimated temperature leads to a five to ten order magnitude change in mantle viscosity (see Figures S6–S8 in Supporting Information S1). However, this value is still higher than 10^{23} Pa, which results in a more elastic response to external loading and has a limited impact on the viscous response of GIA. Nevertheless, the composition variation significantly impacts the resolved lithosphere thickness, which is an important factor in constraining the elastic response of GIA effects.

7. Conclusion

In this study, we applied a new two stage modeling framework to model the mantle thermal and composition structures of Antarctica. We have shown that the compositional variation is required to fully characterize the lithospheric mantle in East Antarctica.

Differences in density, composition, and temperature are modeled between East Antarctica and West Antarctica. In West Antarctica, the lithosphere is less than 100 km thick with a high temperature. The low seismic velocity in these regions is mainly influenced by the temperature. In contrast, the East Antarctic lithosphere is cold and thick. The high depletion in iron content and higher olivine proportion are required to match the extremely fast seismic velocity.

Central East Antarctica and Princess Elizabeth Land characterize high depletion and low temperatures. Based on the Mg#, a depleted Archean-type lithosphere best fits the modeled temperature and composition in these areas. The less depleted lithosphere is located in the Lambert Graben and in the Dronning Maud Land. The less depletion in Lambert Graben might link to the rifting process in the Cretaceous (Lisker et al., 2003). In Dronning Maud Land, TOAST might extend from the coast region to 80°S with a uniformly less depleted mantle (Jacobs et al., 2015; Ruppel et al., 2018). The low Mg# in the TOAST region suggests a Phanerozoic to early Neoproterozoic juvenile crust in this region.

Incorporating compositional changes into the temperature calculations raised the final temperatures by up to 200°C in East Antarctica with a depleted mantle. The updated temperature field is used to calculate lithosphere thickness, heat flow, and mantle viscosity. Our result shows the Amundsen embayment, characterized by low mantle viscosity. Several relatively low-viscosity regions are also modeled in East Antarctica, including the coast region in Wilkes Land. Our model also resolves GHF variation in East Antarctica, showing that considering

compositional variation in the mantle is a necessary step forward to fully characterize fine-scale GHF for ice sheet modeling input. These spatial variables of mantle viscosity and heat flow suggest a complex distribution of bedrock uplift rate and basal boundary conditions for the East Antarctic Ice Sheet.

Data Availability Statement

The model of Antarctic lithosphere is available in Zenodo repository (Li et al., 2024a) and code for generate Antarctic lithosphere is available in Li et al. (2024b).

The seismic velocity model ANT-20 (Lloyd et al., 2020) can be found in <https://ds.iris.edu/ds/products/emc-ant-20/>; Input crust model can be found in Li and Aitken (2023). BedMachine Antarctica V3 can be found by Morlighem (2022). The original data and code of BANCAL22 can be access from Hazzard (2023). Gravity inversion software esys-escript v6.0 can be access from Gross et al. (2023). Figures use Perceptually Uniform Color Maps from ColorCET (Kovesi, 2015).

Acknowledgments

This research was supported by the Australian Research Council Special Research Initiative, Australian Centre for Excellence in Antarctic Science (SR200100008), L.L. was supported by China Scholarship Council–The University of Western Australia joint PhD scholarship (201806170054). We thank Adam Ellery for his help in setting up esys-escript. This work was supported by resources provided by the Pawsey Supercomputing Research Centre (<https://ror.org/04f2f0537>) with funding from the Australian Government and the Government of Western Australia. This work was also supported by the Adapter Allocation Scheme, with computational resources provided by NCI Australia, an NCRIS enabled capability supported by the Australian Government. We thank editor Shin-Chan Han for handling our work and insightful reviews from Douglas Wiens and one anomalous reviewer to great improve the manuscript. We thank Jörg Ebbing and Kirsty Tinto for their constructive comments on an earlier version of the manuscript. We also thank James Hazzard for making BANCAL22 tool public available.

References

- Afonso, J. C., Ben-Mansour, W., O'Reilly, S. Y., Griffin, W. L., Salajegheh, F., Foley, S., et al. (2022). Thermochemical structure and evolution of cratonic lithosphere in central and southern Africa. *Nature Geoscience*, 15(5), 405–410. <https://doi.org/10.1038/s41561-022-00929-y>
- Afonso, J. C., Fullea, J., Yang, Y., Connolly, J. A. D., & Jones, A. G. (2013). 3-D multi-observable probabilistic inversion for the compositional and thermal structure of the lithosphere and upper mantle. II: General methodology and resolution analysis. *Journal of Geophysical Research: Solid Earth*, 118(4), 1650–1676. <https://doi.org/10.1002/jgrb.50123>
- Afonso, J. C., Rawlinson, N., Yang, Y., Schutt, D. L., Jones, A. G., Fullea, J., & Griffin, W. L. (2016). 3-D multiobservable probabilistic inversion for the compositional and thermal structure of the lithosphere and upper mantle: III. Thermochemical tomography in the western-central US. *Journal of Geophysical Research: Solid Earth*, 121(10), 7337–7370. <https://doi.org/10.1002/2016jb013049>
- Afonso, J. C., & Schutt, D. L. (2012). The effects of polybaric partial melting on density and seismic velocities of mantle restites. *Lithos*, 134, 289–303. <https://doi.org/10.1016/j.lithos.2012.01.009>
- Aitken, A., Altinay, C., & Gross, L. (2015). Australia's lithospheric density field, and its isostatic equilibration. *Geophysical Journal International*, 203(3), 1961–1976. <https://doi.org/10.1093/gji/ggv396>
- Aitken, A., Betts, P., Young, D., Blankenship, D. D., Roberts, J., & Siegert, M. J. (2016). The australo-Antarctic Columbia to Gondwana transition. *Gondwana Research*, 29(1), 136–152. <https://doi.org/10.1016/j.gr.2014.10.019>
- Aitken, A. R., Young, D. A., Ferraccioli, F., Betts, P. G., Greenbaum, J. S., Richter, T. G., et al. (2014). The subglacial geology of Wilkes land, East Antarctica. *Geophysical Research Letters*, 41(7), 2390–2400. <https://doi.org/10.1002/2014GL059405>
- Aitken, A. R. A., Li, L., Kulessa, B., Schroeder, D., Jordan, T. A., Whittaker, J. M., et al. (2023). Antarctic sedimentary basins and their influence on ice-sheet dynamics. *Reviews of Geophysics*, 61(3), e2021RG000767. <https://doi.org/10.1029/2021RG000767>
- An, M., Wiens, D. A., Zhao, Y., Feng, M., Nyblade, A. A., Kanao, M., et al. (2015). Temperature, lithosphere–asthenosphere boundary, and heat flux beneath the Antarctic Plate inferred from seismic velocities. *Journal of Geophysical Research: Solid Earth*, 120(12), 8720–8742. <https://doi.org/10.1002/2015jb019197>
- Barletta, V. R., Bevis, M., Smith, B. E., Wilson, T., Brown, A., Bordoni, A., et al. (2018). Observed rapid bedrock uplift in amundsen sea embayment promotes ice-sheet stability. *Science*, 360(6395), 1335–1339. <https://doi.org/10.1126/science.aoa1447>
- Boger, S. D. (2011). Antarctica—Before and after Gondwana. *Gondwana Research*, 19(2), 335–371. <https://doi.org/10.1016/j.gr.2010.09.003>
- Burgos, G., Montagner, J. P., Beucler, E., Capdeville, Y., Mocquet, A., & Drilleau, M. (2014). Oceanic lithosphere–asthenosphere boundary from surface wave dispersion data. *Journal of Geophysical Research: Solid Earth*, 119(2), 1079–1093. <https://doi.org/10.1002/2013jb010528>
- Burton-Johnson, A., Dziadek, R., & Martin, C. (2020). Geothermal heat flow in Antarctica: Current and future directions. *The Cryosphere*, 14(11), 3843–3873. <https://doi.org/10.5194/tc-14-3843-2020>
- Camarano, F., Goes, S., Vacher, P., & Giardini, D. (2003). Inferring upper-mantle temperatures from seismic velocities. *Physics of the Earth and Planetary Interiors*, 138(3–4), 197–222. [https://doi.org/10.1016/s0031-9201\(03\)00156-0](https://doi.org/10.1016/s0031-9201(03)00156-0)
- Codd, A., Gross, L., & Aitken, A. (2021). Fast multi-resolution 3D inversion of potential fields with application to high-resolution gravity and magnetic anomaly data from the Eastern Goldfields in Western Australia. *Computers and Geosciences*, 157, 104941. <https://doi.org/10.1016/j.cageo.2021.104941>
- Cox, S. C., Smith, L. B., & team, T. G. (2019). SCAR GeoMAP dataset (v.201907). [Dataset]. <https://doi.org/10.21420/7SH7-6K05>
- Cox, S. C., Smith Lytle, B., Elkind, S., Smith Siddoway, C., Morin, P., Capponi, G., et al. (2023). A continent-wide detailed geological map dataset of Antarctica. *Scientific Data*, 10(1), 250. <https://doi.org/10.1038/s41597-023-02152-9>
- Dalton, C. A., Langmuir, C. H., & Gale, A. (2014). Geophysical and geochemical evidence for deep temperature variations beneath mid-ocean ridges. *Science*, 344(6179), 80–83. <https://doi.org/10.1126/science.1249466>
- Dalziel, I., & Lawyer, L. (2001). The lithospheric setting of the West Antarctic ice sheet. *The West Antarctic Ice Sheet: Behavior and Environment, Antarctic Research Series*, 77, 29–44. <https://doi.org/10.1029/ar077p0029>
- Dziadek, R., Ferraccioli, F., & Gohl, K. (2021). High geothermal heat flow beneath Thwaites Glacier in West Antarctica inferred from aeromagnetic data. *Communications Earth and Environment*, 2(1), 1–6. <https://doi.org/10.1038/s43247-021-00242-3>
- Feng, M., van der Lee, S., An, M., & Zhao, Y. (2010). Lithospheric thickness, thinning, subduction, and interaction with the asthenosphere beneath China from the joint inversion of seismic S-wave train fits and Rayleigh-wave dispersion curves. *Lithos*, 120(1–2), 116–130. <https://doi.org/10.1016/j.lithos.2009.11.017>
- Ferraccioli, F., Finn, C. A., Jordan, T. A., Bell, R. E., Anderson, L. M., & Damaske, D. (2011). East Antarctic rifting triggers uplift of the Gamburtsev Mountains. *Nature*, 479(7373), 388–392. <https://doi.org/10.1038/nature10566>
- Foulger, G. R., Panza, G. F., Artemieva, I. M., Bastow, I. D., Cammarano, F., Evans, J. R., et al. (2013). Caveats on tomographic images. *Terra Nova*, 25(4), 259–281. <https://doi.org/10.1111/ter.12041>

- Fullea, J., Afonso, J. C., Connolly, J. A. D., Fernandez, M., García-Castellanos, D., & Zeyen, H. (2009). LitMod3D: An interactive 3-D software to model the thermal, compositional, density, seismological, and rheological structure of the lithosphere and sublithospheric upper mantle. *Geochemistry, Geophysics, Geosystems*, 10(8). <https://doi.org/10.1029/2009gc002391>
- Fullea, J., Lebedev, S., Martinec, Z., & Celli, N. L. (2021). WINTERC-G: Mapping the upper mantle thermochemical heterogeneity from coupled geophysical–petrological inversion of seismic waveforms, heat flow, surface elevation and gravity satellite data. *Geophysical Journal International*, 226(1), 146–191. <https://doi.org/10.1093/gji/ggab094>
- Gaul, O. F., Griffin, W. L., O'Reilly, S. Y., & Pearson, N. J. (2000). Mapping olivine composition in the lithospheric mantle. *Earth and Planetary Science Letters*, 182(3–4), 223–235. [https://doi.org/10.1016/s0012-821x\(00\)00243-0](https://doi.org/10.1016/s0012-821x(00)00243-0)
- Geuzaine, C., & Remacle, J. F. (2009). Gmsh: A 3-D finite element mesh generator with built-in pre- and post-processing facilities. *International Journal for Numerical Methods in Engineering*, 79(11), 1309–1331. <https://doi.org/10.1002/nme.2579>
- Goes, S., Govers, R., & Vacher, P. (2000). Shallow mantle temperatures under Europe from P and S wave tomography. *Journal of Geophysical Research: Solid Earth*, 105(B5), 11153–11169. <https://doi.org/10.1029/1999jb900300>
- Gooch, B. T., Young, D. A., & Blankenship, D. D. (2016). Potential groundwater and heterogeneous heat source contributions to ice sheet dynamics in critical submarine basins of East Antarctica. *Geochemistry, Geophysics, Geosystems*, 17(2), 395–409. <https://doi.org/10.1002/2015gc006117>
- Gross, L., Bourguin, L., Hale, A. J., & Mühlhaus, H.-B. (2007). Interface modeling in incompressible media using level sets in Escript. *Physics of the Earth and Planetary Interiors*, 163(1–4), 23–34. <https://doi.org/10.1016/j.pepi.2007.04.004>
- Gross, L., Codd, A., & Ellery, A. (2023). esys-escript 6.0. [Software]. The University of Queensland. <https://doi.org/10.48610/24e6e34>
- Haeger, C., Kaban, M. K., Tesauro, M., Petrunin, A. G., & Mooney, W. D. (2019). 3D density, thermal and compositional model of the Antarctic lithosphere and implications for its evolution. *Geochemistry, Geophysics, Geosystems*, 20(2), 688–707. <https://doi.org/10.1029/2018GC008033>
- Haeger, C., Petrunin, A. G., & Kaban, M. K. (2022). Geothermal heat flow and thermal structure of the Antarctic lithosphere. *Geochemistry, Geophysics, Geosystems*, 23(10), e2022GC010501. <https://doi.org/10.1029/2022gc010501>
- Hazzard, J. A. N. (2023). Code associated with manuscript: "Probabilistic assessment of Antarctic thermomechanical structure: Impacts on ice sheet stability". (v2). Zenodo. [Software]. <https://doi.org/10.5281/zenodo.7970922>
- Hazzard, J. A. N., & Richards, F. D. (2024). Antarctic geothermal heat flow, crustal conductivity and heat production inferred from seismological data. *Geophysical Research Letters*, 51(7), e2023GL106274. <https://doi.org/10.1029/2023gl106274>
- Hazzard, J. A. N., Richards, F. D., Goes, S. D. B., & Roberts, G. G. (2023). Probabilistic assessment of Antarctic thermomechanical structure: Impacts on ice sheet stability. *Journal of Geophysical Research: Solid Earth*, 128(5), e2023JB026653. <https://doi.org/10.1029/2023jb026653>
- Hoggard, M. J., Czarnota, K., Richards, F. D., Huston, D. L., Jaques, A. L., & Ghelichkhan, S. (2020). Global distribution of sediment-hosted metals controlled by craton edge stability. *Nature Geoscience*, 13(7), 504–510. <https://doi.org/10.1038/s41561-020-0593-2>
- Jacobs, J., Elburg, M., Läufer, A., Kleinhanns, I. C., Henjes-Kunst, F., Estrada, S., et al. (2015). Two distinct late Mesoproterozoic/early Neoproterozoic basement provinces in central/eastern Dronning Maud Land, East Antarctica: The missing link, 15–21 E. *Precambrian Research*, 265, 249–272. <https://doi.org/10.1016/j.precamres.2015.05.003>
- Jordan, T. A., Ferraccioli, F., & Forsberg, R. (2022). An embayment in the East Antarctic basement constrains the shape of the Rodinian continental margin. *Communications Earth and Environment*, 3(1), 1–8. <https://doi.org/10.1038/s43247-022-00375-z>
- Jordan, T. A., Ferraccioli, F., Ross, N., Corr, H. F. J., Leat, P. T., Bingham, R. G., et al. (2013). Inland extent of the Weddell Sea Rift imaged by new aerogeophysical data. *Tectonophysics*, 585(C), 137–160. <https://doi.org/10.1016/j.tecto.2012.09.010>
- Jordan, T. A., Riley, T. R., & Siddoway, C. S. (2020). The geological history and evolution of West Antarctica. *Nature Reviews Earth and Environment*, 1(2), 117–133. <https://doi.org/10.1038/s43017-019-0013-6>
- Kaban, M. K., Tesauro, M., Mooney, W. D., & Cloetingh, S. A. P. L. (2014). Density, temperature, and composition of the North American lithosphere—New insights from a joint analysis of seismic, gravity, and mineral physics data: I. Density structure of the crust and upper mantle. *Geochemistry, Geophysics, Geosystems*, 15(12), 4781–4807. <https://doi.org/10.1029/2014gc005483>
- Karato, S.-i., & Jung, H. (1998). Water, partial melting and the origin of the seismic low velocity and high attenuation zone in the upper mantle. *Earth and Planetary Science Letters*, 157(3–4), 193–207. [https://doi.org/10.1016/s0012-821x\(98\)00034-x](https://doi.org/10.1016/s0012-821x(98)00034-x)
- Katz, R. F., Spiegelman, M., & Langmuir, C. H. (2003). A new parameterization of hydrous mantle melting. *Geochemistry, Geophysics, Geosystems*, 4(9). <https://doi.org/10.1029/2002gc000433>
- Kovesi, P. (2015). Good colour maps: How to design them. *arXiv preprint arXiv:1509.03700*.
- Kustowski, B., Ekström, G., & Dziewoński, A. (2008). Anisotropic shear-wave velocity structure of the Earth's mantle: A global model. *Journal of Geophysical Research*, 113(B6). <https://doi.org/10.1029/2007jb005169>
- Kvas, A., Mayer-Gürr, T., Krauss, S., Brockmann, J. M., Schubert, T. S., Wolf-Dieter, et al. (2019). The satellite-only gravity field model GOCO06s. [Dataset]. <https://doi.org/10.5880/ICGEM.2019.002>
- Li, L., & Aitken, A. (2023). Antarctic crustal Model and radiogenic heat production. [Dataset]. <https://doi.org/10.5281/zenodo.10242299>
- Li, L., Aitken, A., Gross, L., & Codd, A. (2024a). Antarctic lithosphere model. [Dataset]. <https://doi.org/10.5281/zenodo.11516434>
- Li, L., Aitken, A., Gross, L., & Codd, A. (2024b). Source code for Antarctic lithosphere. (V1.0). Zenodo. [Software]. <https://doi.org/10.5281/zenodo.11516393>
- Li, L., Aitken, A. R., Lindsay, M. D., & Kulessa, B. (2022). Sedimentary basins reduce stability of Antarctic ice streams through groundwater feedbacks. *Nature Geoscience*, 15(8), 645–650. <https://doi.org/10.1038/s41561-022-00992-5>
- Li, L., & Aitken, A. R. A. (2024). Crustal heterogeneity of Antarctica signals spatially variable radiogenic heat production. *Geophysical Research Letters*, 51(2), e2023GL106201. <https://doi.org/10.1029/2023gl106201>
- Lisker, F., Brown, R., & Fabel, D. (2003). Denudational and thermal history along a transect across the Lambert Graben, northern Prince Charles Mountains, Antarctica, derived from apatite fission track thermochronology. *Tectonics*, 22(5). <https://doi.org/10.1029/2002tc001477>
- Lloyd, A. J., Wiens, D. A., Zhu, H., Tromp, J., Nyblade, A. A., Aster, R. C., et al. (2020). Seismic structure of the Antarctic upper mantle imaged with adjoint tomography. *Journal of Geophysical Research: Solid Earth*, 125(3). <https://doi.org/10.1029/2019jb017823>
- Clubes, M., Lanseau, C., & Rémy, F. (2006). Relations between basal condition, subglacial hydrological networks and geothermal flux in Antarctica. *Earth and Planetary Science Letters*, 241(3–4), 655–662. <https://doi.org/10.1016/j.epsl.2005.10.040>
- Lösing, M., & Ebbing, J. (2021). Predicting geothermal heat flow in Antarctica with a machine learning approach. *Journal of Geophysical Research: Solid Earth*, 126(6), e2020JB021499. <https://doi.org/10.1029/2020jb021499>
- Maaløe, S., & Aoki, K.-i. (1977). The major element composition of the upper mantle estimated from the composition of lherzolites. *Contributions to Mineralogy and Petrology*, 63(2), 161–173. <https://doi.org/10.1007/bf00398777>

- Manassero, M. C., Özaydin, S., Afonso, J. C., Shea, J. J., Ezad, I. S., Kirkby, A., et al. (2024). Lithospheric structure and melting processes in southeast Australia: New constraints from joint probabilistic inversions of 3D magnetotelluric and seismic data. *Journal of Geophysical Research: Solid Earth*, 129(3), e2023JB028257. <https://doi.org/10.1029/2023jb028257>
- Martin, A. P. (2023). A review of the composition and chemistry of peridotite mantle xenoliths in volcanic rocks from Antarctica and their relevance to petrological and geophysical models for the lithospheric mantle. *Geological Society, London, Memoirs*, 56(1), 343–354. <https://doi.org/10.1144/m56-2021-26>
- Martos, Y. M., Catalán, M., Jordan, T. A., Golynsky, A., Golynsky, D., Eagles, G., & Vaughan, D. G. (2017). Heat flux distribution of Antarctica unveiled. *Geophysical Research Letters*, 44(22), 11417–11426. <https://doi.org/10.1002/2017gl075609>
- McCormack, F. S., Roberts, J. L., Dow, C. F., Stål, T., Halpin, J. A., Reading, A. M., & Siegert, M. J. (2022). Fine-scale geothermal heat flow in Antarctica can increase simulated subglacial melt estimates. *Geophysical Research Letters*, 49(15), e2022GL098539. <https://doi.org/10.1029/2022gl098539>
- McDonough, W. F., & Sun, S. S. (1995). The composition of the Earth. *Chemical Geology*, 120(3–4), 223–253. [https://doi.org/10.1016/0009-2541\(94\)00140-4](https://doi.org/10.1016/0009-2541(94)00140-4)
- McDonough, W. s. (1990). Constraints on the composition of the continental lithospheric mantle. *Earth and Planetary Science Letters*, 101(1), 1–18. [https://doi.org/10.1016/0012-821x\(90\)90119-i](https://doi.org/10.1016/0012-821x(90)90119-i)
- McKenzie, D., Jackson, J., & Priestley, K. (2005). Thermal structure of oceanic and continental lithosphere. *Earth and Planetary Science Letters*, 233(3–4), 337–349. <https://doi.org/10.1016/j.epsl.2005.02.005>
- Morlighem, M. (2022). MEaSUREs BedMachine Antarctica (V3). [Dataset]. <https://doi.org/10.5067/FPSU0V1MWUB6>
- Morlighem, M., Rignot, E., Binder, T., Blankenship, D., Drews, R., Eagles, G., et al. (2020). Deep glacial troughs and stabilizing ridges unveiled beneath the margins of the Antarctic ice sheet. *Nature Geoscience*, 13(2), 132–137. <https://doi.org/10.1038/s41561-019-0510-8>
- Nield, G. A., Barletta, V. R., Bordoni, A., King, M. A., Whitehouse, P. L., Clarke, P. J., et al. (2014). Rapid bedrock uplift in the Antarctic Peninsula explained by viscoelastic response to recent ice unloading. *Earth and Planetary Science Letters*, 397, 32–41. <https://doi.org/10.1016/j.epsl.2014.04.019>
- Nield, G. A., Whitehouse, P. L., King, M. A., & Clarke, P. J. (2016). Glacial isostatic adjustment in response to changing Late Holocene behaviour of ice streams on the Siple Coast, West Antarctica. *Geophysical Supplements to the Monthly Notices of the Royal Astronomical Society*, 205(1), 1–21. <https://doi.org/10.1093/gji/ggv532>
- Noble, T. L., Rohling, E. J., Aitken, A. R. A., Bostock, H. C., Chase, Z., Gomez, N., et al. (2020). The sensitivity of the Antarctic ice sheet to a changing climate: Past, present, and future. *Reviews of Geophysics*, 58(4). <https://doi.org/10.1029/2019RG000663>
- Pappa, F., Ebbing, J., Ferraccioli, F., & van der Wal, W. (2019). Modeling satellite gravity gradient data to derive density, temperature, and viscosity structure of the Antarctic lithosphere. *Journal of Geophysical Research: Solid Earth*, 124(11), 12053–12076. <https://doi.org/10.1029/2019jb017997>
- Priestley, K., & McKenzie, D. (2006). The thermal structure of the lithosphere from shear wave velocities. *Earth and Planetary Science Letters*, 244(1–2), 285–301. <https://doi.org/10.1016/j.epsl.2006.01.008>
- Ramirez, F. D. C., Selway, K., Conrad, C. P., & Lithgow-Bertelloni, C. (2022). Constraining upper mantle viscosity using temperature and water content inferred from seismic and magnetotelluric data. *Journal of Geophysical Research: Solid Earth*, 127(8), e2021JB023824. <https://doi.org/10.1029/2021jb023824>
- Reading, A. M., Stål, T., Halpin, J. A., Lösing, M., Ebbing, J., Shen, W., et al. (2022). Antarctic geothermal heat flow and its implications for tectonics and ice sheets. *Nature Reviews Earth and Environment*, 3(12), 814–831. <https://doi.org/10.1038/s43017-022-00348-y>
- Richards, F., Hoggard, M., Cowton, L., & White, N. (2018). Reassessing the thermal structure of oceanic lithosphere with revised global inventories of basement depths and heat flow measurements. *Journal of Geophysical Research: Solid Earth*, 123(10), 9136–9161. <https://doi.org/10.1029/2018jb015998>
- Richards, F. D., Hoggard, M. J., White, N., & Ghelichkhan, S. (2020). Quantifying the relationship between short-wavelength dynamic topography and thermomechanical structure of the upper mantle using calibrated parameterization of anelasticity. *Journal of Geophysical Research: Solid Earth*, 125(9), e2019JB019062. <https://doi.org/10.1029/2019jb019062>
- Rignot, E., Mouginot, J., Scheuchl, B., van den Broeke, M., van Wessem, M. J., & Morlighem, M. (2019). Four decades of Antarctic ice sheet mass balance from 1979–2017. *Proceedings of the National Academy of Sciences of the United States of America*, 116(4), 1095–1103. <https://doi.org/10.1073/pnas.1812883116>
- Ruppel, A., Jacobs, J., Eagles, G., Läufer, A., & Jokat, W. (2018). New geophysical data from a key region in East Antarctica: Estimates for the spatial extent of the Tonian Oceanic Arc Super terrane (TOAST). *Gondwana Research*, 59, 97–107. <https://doi.org/10.1016/j.gr.2018.02.019>
- Schaar, R., Gross, L., & Du Plessis, J. (2016). PDE-Based geophysical modelling using finite elements: Examples from 3D resistivity and 2D magnetotellurics. *Journal of Geophysics and Engineering*, 13(2), S59–S73. <https://doi.org/10.1088/1742-2132/13/2/s59>
- Schaeffer, A., & Lebedev, S. (2015). Global heterogeneity of the lithosphere and underlying mantle: A seismological appraisal based on multimode surface-wave dispersion analysis, shear-velocity tomography, and tectonic regionalization. In *The Earth's heterogeneous mantle* (pp. 3–46). Springer.
- Scheinert, M., Ferraccioli, F., Schwabe, J., Bell, R., Studinger, M., Damaske, D., et al. (2016). New Antarctic gravity anomaly grid for enhanced geodetic and geophysical studies in Antarctica. *Geophysical Research Letters*, 43(2), 600–610. <https://doi.org/10.1002/2015GL067439>
- Schroeder, D. M., Blankenship, D. D., Young, D. A., & Quartini, E. (2014). Evidence for elevated and spatially variable geothermal flux beneath the West Antarctic Ice Sheet. *Proceedings of the National Academy of Sciences of the United States of America*, 111(25), 9070–9072. <https://doi.org/10.1073/pnas.1405184111>
- Schutt, D. L., & Lesher, C. E. (2006). Effects of melt depletion on the density and seismic velocity of garnet and spinel lherzolite. *Journal of Geophysical Research*, 111(B5). <https://doi.org/10.1029/2003jb002950>
- Shen, W., Wiens, D., Anandakrishnan, S., Aster, R., Gerstoft, P., Bromirski, P., et al. (2018). The crust and upper mantle structure of central and WestWest Antarctica from Bayesian inversion of Rayleigh wave and receiver functions. *Journal of Geophysical Research: Solid Earth*, 123(9), 7824–7849. <https://doi.org/10.1029/2017jb015346>
- Shen, W., Wiens, D. A., Lloyd, A. J., & Nyblade, A. A. (2020). A geothermal heat flux map of Antarctica empirically constrained by seismic structure. *Geophysical Research Letters*, 47(14), e2020GL086955. <https://doi.org/10.1029/2020gl086955>
- Shorttle, O., MacLennan, J., & Lambart, S. (2014). Quantifying lithological variability in the mantle. *Earth and Planetary Science Letters*, 395, 24–40. <https://doi.org/10.1016/j.epsl.2014.03.040>
- Siddoway, C. (2008). Tectonics of the West Antarctic Rift System: New light on the history and dynamics of distributed intracontinental extension. In *Antarctica: A keystone in a changing world* (pp. 91–114).
- Stål, T., Reading, A. M., Halpin, J. A., & Whittaker, J. M. (2019). A multivariate approach for mapping lithospheric domain boundaries in East Antarctica. *Geophysical Research Letters*, 46(17–18), 10404–10416. <https://doi.org/10.1029/2019gl083453>

- Stål, T., Reading, A. M., Halpin, J. A., & Whittaker, J. M. (2021). Antarctic geothermal heat flow model: Aq1. *Geochemistry, Geophysics, Geosystems*, 22(2), e2020GC009428. <https://doi.org/10.1029/2020gc009428>
- Stixrude, L., & Lithgow-Bertelloni, C. (2005). Thermodynamics of mantle minerals—I. Physical properties. *Geophysical Journal International*, 162(2), 610–632. <https://doi.org/10.1111/j.1365-246x.2005.02642.x>
- Stixrude, L., & Lithgow-Bertelloni, C. (2011). Thermodynamics of mantle minerals-II. Phase equilibria. *Geophysical Journal International*, 184(3), 1180–1213. <https://doi.org/10.1111/j.1365-246x.2010.04890.x>
- Sun, S. S., & McDonough, W. F. (1989). Chemical and isotopic systematics of oceanic basalts: Implications for mantle composition and processes. *Geological Society*, 42(1), 313–345. <https://doi.org/10.1144/gsl.sp.1989.042.01.19>
- Tankersley, M. D., Horgan, H. J., Siddoway, C. S., Tontini, F. C., & Tinto, K. J. (2022). Basement topography and sediment thickness beneath Antarctica's Ross Ice Shelf. *Geophysical Research Letters*, 49(10), e2021GL097371. <https://doi.org/10.1029/2021gl097371>
- Tesauro, M., Kaban, M. K., Mooney, W. D., & Cloetingh, S. A. P. L. (2014). Density, temperature, and composition of the North American lithosphere—New insights from a joint analysis of seismic, gravity, and mineral physics data: 2. Thermal and compositional model of the upper mantle. *Geochemistry, Geophysics, Geosystems*, 15(12), 4808–4830. <https://doi.org/10.1002/2014gc005484>
- Tinto, K. J., Padman, L., Siddoway, C. S., Springer, S. R., Fricker, H. A., Das, I., et al. (2019). Ross Ice Shelf response to climate driven by the tectonic imprint on seafloor bathymetry. *Nature Geoscience*, 12(6), 441–449. <https://doi.org/10.1038/s41561-019-0370-2>